

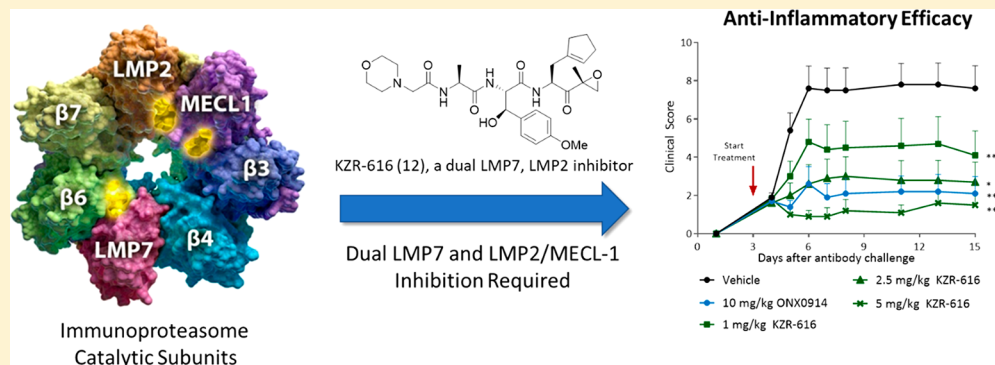
Required Immunoproteasome Subunit Inhibition Profile for Anti-Inflammatory Efficacy and Clinical Candidate KZR-616 ((2*S*,3*R*)-*N*-((*S*)-3-(Cyclopent-1-en-1-yl)-1-((*R*)-2-methyloxiran-2-yl)-1-oxopropan-2-yl)-3-hydroxy-3-(4-methoxyphenyl)-2-((*S*)-2-(2-morpholinoacetamido)propanamido)propenamido)

Henry W. B. Johnson,[†] Eric Lowe,[†] Janet L. Anderl,[†] Andrea Fan,[†] Tony Muchamuel,[†] Simeon Bowers,[‡] David C. Moebius,[‡] Christopher Kirk,[†] and Dustin L. McMinn^{*,†,§}

[†]Kezar Life Sciences, 4000 Shoreline Court, Suite 300, South San Francisco, California 94080, United States

[‡]Onyx Pharmaceuticals, an Amgen Subsidiary, South San Francisco, California 94080, United States

Supporting Information



ABSTRACT: Selective immunoproteasome inhibition is a promising approach for treating autoimmune disorders, but optimal proteolytic active site subunit inhibition profiles remain unknown. We reveal here our design of peptide epoxyketone-based selective low molecular mass polypeptide-7 (LMP7) and multicatalytic endopeptidase complex subunit-1 (MECL-1) subunit inhibitors. Utilizing these and our previously disclosed low molecular mass polypeptide-2 (LMP2) inhibitor, we demonstrate a requirement of dual LMP7/LMP2 or LMP7/MECL-1 subunit inhibition profiles for potent cytokine expression inhibition and in vivo efficacy in an inflammatory disease model. These and additional findings toward optimized solubility led the design and selection of KZR-616 disclosed here and presently in clinical trials for treatment of rheumatic disease.

INTRODUCTION

Proteasomes control several cellular processes by mediating protein homeostasis through regulated protein degradation.¹ Proteasome function is tuned between a ubiquitously expressed constitutive proteasome and an immuno-optimized form, or immunoproteasome, largely confined to cells of hematopoietic origin or induced elsewhere by inflammatory cytokines. These isoforms further differ by subtle sequence differences in proteolytic subunits of their 20S core particles (Figure 1). The constitutive proteasome contains two copies each of three proteolytic subunits within its 20S core, β 1, β 2, and β 5, while the immunoproteasome replaces these with low-molecular mass polypeptide-2 (LMP2 or β 1i), multicatalytic endopeptidase complex-like 1 (MECL-1 or β 2i), and low-molecular mass polypeptide-7 (LMP7 or β 5i), respectively. Sequence differences between analogous subunits render altered substrate preferences and engender specialized roles for the immunoproteasome (antigen presentation, cytokine

regulation, etc.).² Increased expression of the immunoproteasome is observed at sites of inflammation in several autoimmune disorders.^{3–5}

Combined inhibition of both forms of the proteasome, specifically the β 5 and LMP7 subunits, drives cell death and has been an effective drug strategy against multiple myeloma,⁶ but chronic administration in non-life-threatening disorders, such as autoimmunity, is precluded by systemic toxicities including anemia, thrombocytopenia, and neutropenia.⁷ Nonetheless, bortezomib, a dual proteasome inhibitor, demonstrated efficacy in mouse models of autoimmunity and resulted in improved clinical outcomes in patients with systemic lupus erythematosus^{8–10} and other autoimmune disorders.^{11,12}

ONX 0914 (Figure 2), a peptide epoxyketone-based immunoproteasome-selective inhibitor, potently blocks inflam-

Received: July 31, 2018

Published: October 31, 2018

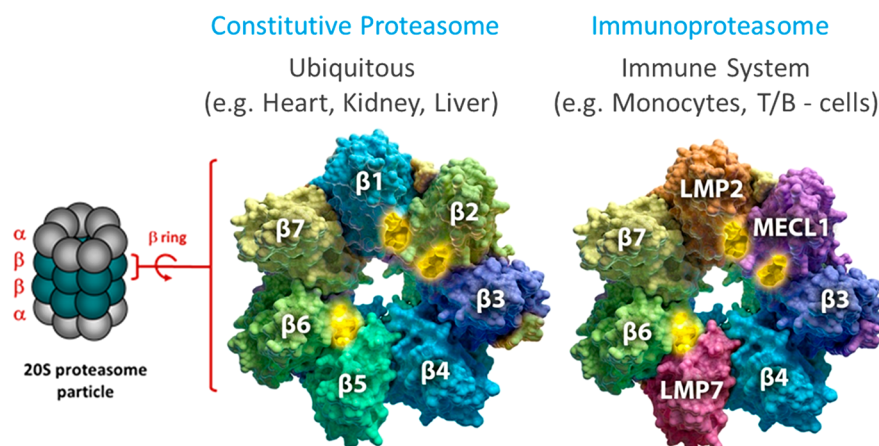


Figure 1. Subunit composition of the proteasome 20S core particle β rings.

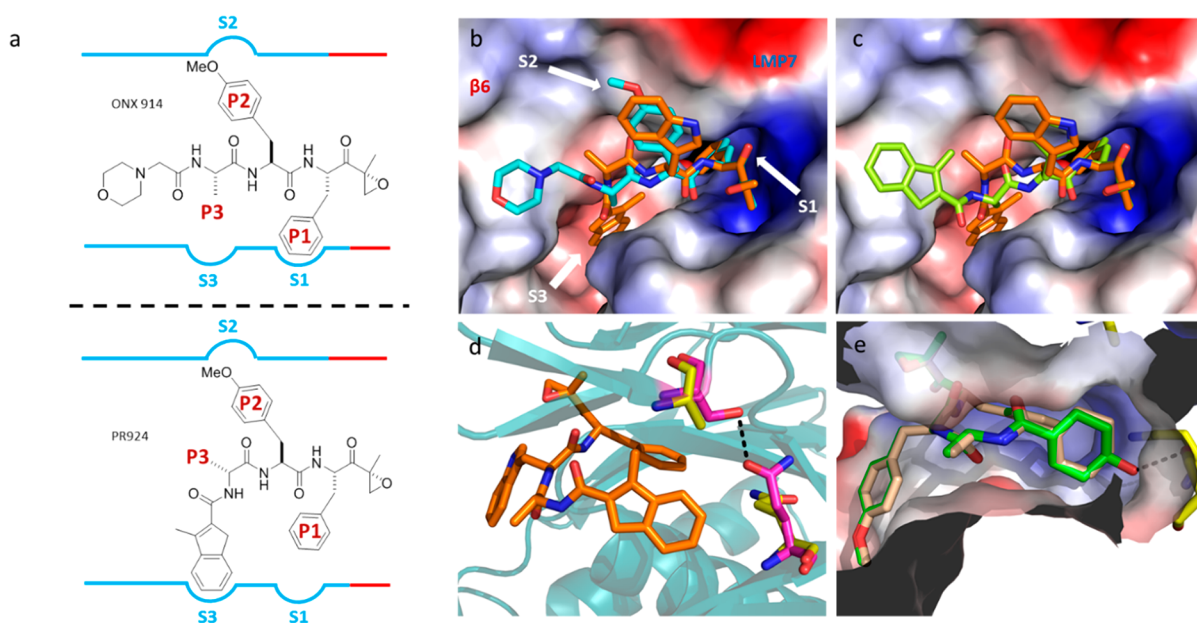


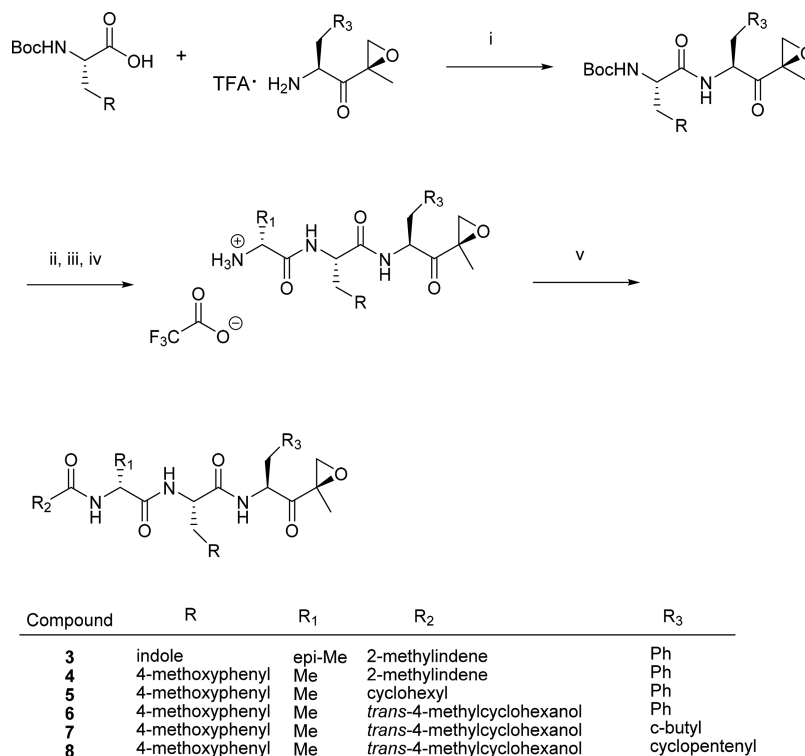
Figure 2. Modeling of selective inhibitors within the human LMP7/ β 6 binding site. (a) ONX 914 and PR-924 registered to selectivity pockets. (b) Different binding modes are observed for PR-924 (orange) and ONX 914 (blue) (van der Waals surfaces). (c) PR-924 (orange) and the P3 epimer, **3** (green). (d) PR-924 modeled with Ala28 and Glu131 residues highlighted (yellow). In human β 5 (magenta) and mouse (not shown for clarity), an H-bonding interaction between Glu131 and Ser28 is observed. (e) Cutaway of the S3 pocket with the cyclohexyl P3 analogue, **5**, and the *trans* cyclohexanol, **6**, superimposed.

matory cytokine production and alters proinflammatory T-cell plasticity without the antiproliferative effects of nonselective proteasome inhibitors.¹³ Moreover, ONX 914 is efficacious in animal models of autoimmune disease (rheumatoid arthritis, type I diabetes, multiple sclerosis,¹⁴ colitis,¹⁵ and lupus¹⁶) and results in no loss of normal immune function. At effective doses, ONX 914 maximally inhibited mouse LMP7 while sparing constitutive proteasome subunit activity.¹³ Though these results suggested LMP7 was the primary therapeutic target, efficacious doses were associated with 60% inhibition of LMP2 and a low level of MECL-1 inhibition. Moreover, partial LMP2/MECL-1 inhibition by ONX 914 in stimulated T-cells enhanced *in vitro* cytokine inhibition.¹³ Together, these observations suggested the anti-inflammatory effects of ONX 914 may be potentiated by LMP2 and/or MECL-1 inhibition, an implication that we sought to clarify through design and assessment of epoxyketone-based selective inhibitors to each of the immunoproteasome subunits.

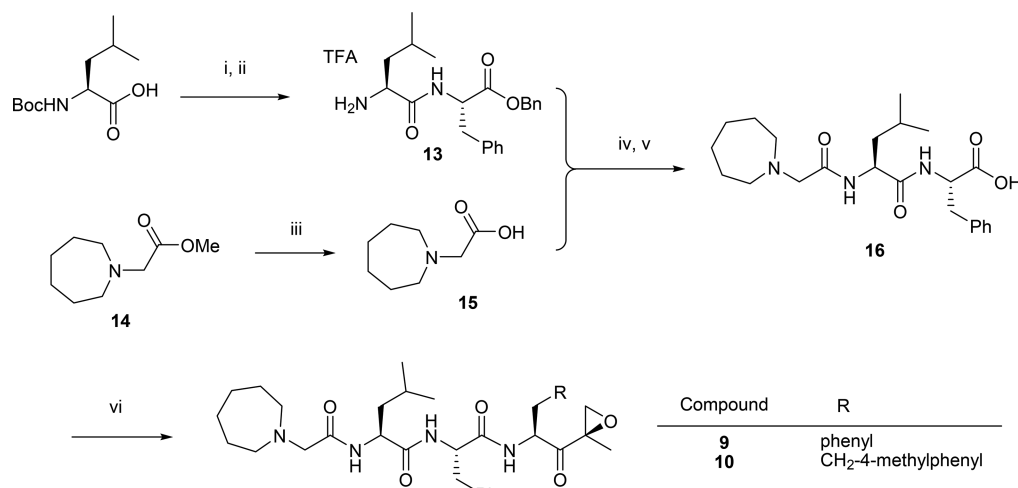
RESULTS AND DISCUSSION

Chemistry. The generation of LMP7 inhibitors **3–8** (Scheme 1) involved standard peptide coupling chemistry and commenced with the coupling of the BOC protected amino acid with the appropriate keto-epoxide TFA salt. The dipeptide building block was then deprotected and coupled to D- or L-BOC protected alanine to furnish the BOC intermediate. After deprotection the TFA salt was carried into a final amide coupling step.

The synthesis of MECL-1 inhibitors (Scheme 2) started with a coupling of BOC-leucine to L-phenylalanine benzyl ester followed by a deprotection to furnish the TFA salt (**13**). The N-cap was synthesized by hydrolyzing methyl 2-(azepan-1-yl)acetate (**14**) to provide the corresponding acid (**15**). Coupling of **13** and **15** yielded the dipeptide for which the benzyl ester was cleaved by hydrogenation to yield **16**. Final coupling of the corresponding keto-epoxide TFA salt using HATU furnished the MECL-1 inhibitors **9** and **10**.

Scheme 1^a

^aReagents and conditions: (i) hydroxybenzotriazole, 2-(1*H*-benzotriazol-1-yl)-1,1,3,3-tetramethyluronium hexafluorophosphate (HBTU), *N*-ethyl-*N*-isopropylpropan-2-amine, DMF, 0 °C → rt; (ii) TFA, DCM; (iii) (*tert*-butoxycarbonyl)-*L*-alanine or (*tert*-butoxycarbonyl)-*D*-alanine, 1-[bis(dimethylamino)methylene]-1*H*-1,2,3-triazolo[4,5-*b*]pyridinium 3-oxide hexafluorophosphate (HATU), *N*-ethyl-*N*-isopropylpropan-2-amine, DMF, 0 °C → rt; (iv) TFA, DCM; (v) R₂-COOH, HATU, *N*-ethyl-*N*-isopropylpropan-2-amine, DMF, 0 °C → rt.

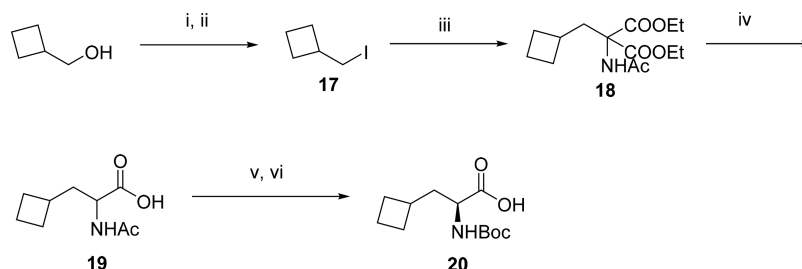
Scheme 2^a

^aReagents and conditions: (i) *L*-phenylalanine benzyl ester, 1-[bis(dimethylamino)methylene]-1*H*-1,2,3-triazolo[4,5-*b*]pyridinium 3-oxide hexafluorophosphate (HATU), *N*-ethyl-*N*-isopropylpropan-2-amine, DMF, 0 °C → rt (84%); (ii) TFA, DCM, 0 °C → rt (quant); (iii) methyl 2-(azepan-1-yl)acetate, LiOH-H₂O; (iv) HATU, *N*-ethyl-*N*-isopropylpropan-2-amine, DMF, 0 °C → rt (90% over 2 steps); (v) Pd/C (10%), methanol, H₂ (quant); (vi) (*S*)-2-amino-1-((*R*)-2-methyloxiran-2-yl)-3-phenylpropan-1-one TFA salt or **24**, HATU, *N*-ethyl-*N*-isopropylpropan-2-amine, DMF, 0 °C → rt.

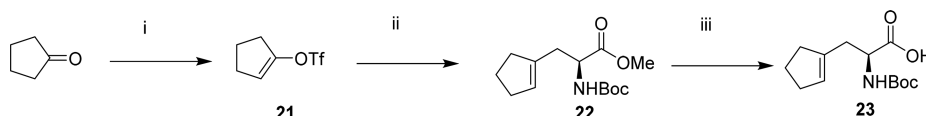
The custom amino acids required for P1 keto-epoxide building blocks involved two different routes. The cyclobutylamino acid started with cyclobutylmethanol and in two steps was converted to the corresponding iodide (Scheme 3, **17**). Condensation with diethyl 2-acetamidomalonnate provided the corresponding diester (**18**) which was hydrolyzed to

provide racemic **19**. An enzymatic resolution with *L*-acylase provided the *S*-enantiomer of the amino acid which was directly BOC protected to yield the amino acid **20**.

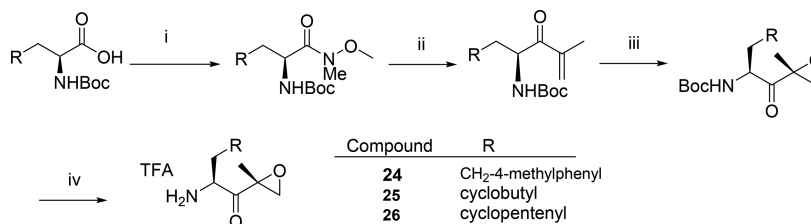
An alternative route toward the cyclopentylamino acid was also employed (Scheme 4). Cyclopentanone was treated with triflic anhydride and sodium carbonate to provide **21**. The

Scheme 3^a

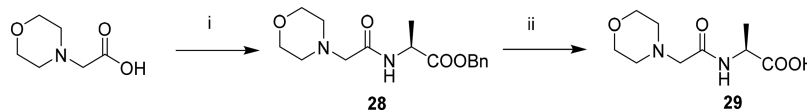
^aReagents and conditions: (i) methanesulfonyl chloride, cyclobutylmethanol, triethylamine, DCM, 0 °C → rt; (ii) sodium iodide, methanesulfonate, acetone; (iii) potassium *tert*-butoxide, diethyl 2-acetamidomalonate, DMF; (iv) ethanol, NaOH (34% over 4 steps); (v) L-acylase, water, 37 °C; (vi) BOC₂O, NaOH (47% over 2 steps).

Scheme 4^a

^aReagents and conditions: (i) trifluoromethanesulfonic anhydride, sodium carbonate, DCM, -20 °C → rt (73%); (ii) methyl (*R*)-2-((*tert*-butoxycarbonyl)amino)-3-iodopropanoate, Zn dust, trimethylsilyl chloride, [1,1'-bis(diphenylphosphino)ferrocene]dichloropalladium(II), DMF, 0 °C → 50 °C (72%); (iii) LiOH, water, methanol (95%).

Scheme 5^a

^aReagents and conditions: (i) *N,O*-dimethylhydroxylamine hydrochloride, ethyl chloroformate, *N*-methylmorpholine, THF, DCM, 0 °C → rt; (ii) isopropenylmagnesium bromide, THF, 0 °C; (iii) sodium hypochlorite, DMF, -20 °C → 0 °C; (iv) TFA, DCM.

Scheme 6^a

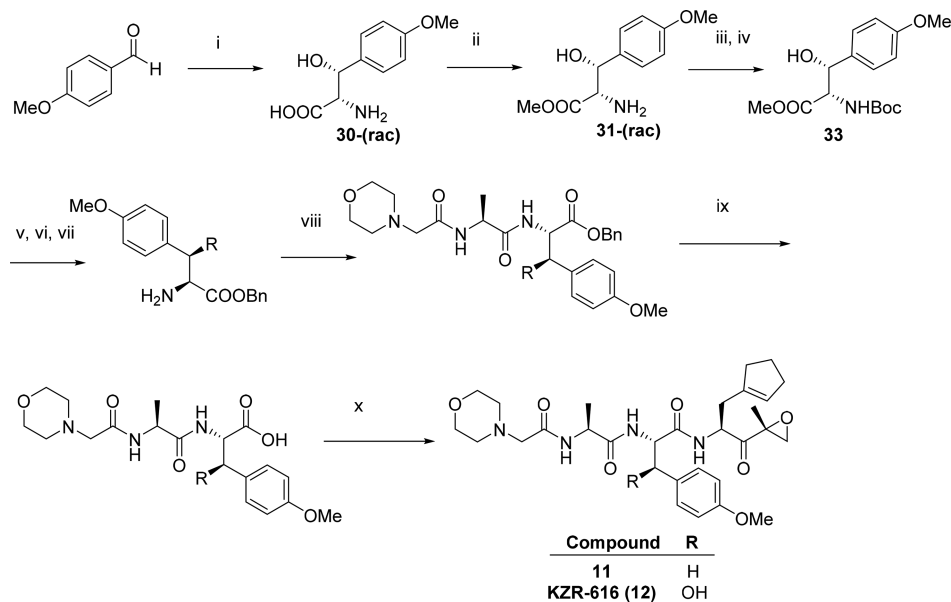
^aReagents and conditions: (i) benzyl *L*-alaninate, 4-(4,6-dimethoxy-1,3,5-triazin-2-yl)-4-methylmorpholinium chloride (DMTMM), *N*-methylmorpholine, DMF, DCM (50%); (ii) hydrogen, Pd/C (10%), THF (86%).

crude vinyl triflate was carried directly into a Negishi coupling with diprotected alkyl iodide. The fully protected amino acid **22** was then hydrolyzed to provide **23**.

Synthesis of the keto-epoxides involved a four-step sequence starting from the requisite BOC protected amino acids (Scheme 5). Weinreb amide formation followed by addition of isopropenylmagnesium bromide provided the enone in high yield. Addition of bleach resulted in rapid conversion to the epoxide. Removal of the BOC group yielded the labile amine TFA salt which was carried forward directly without further purification.

The synthesis of **11** and KZR-616 (**12**) employed the same P3/*N*-cap building block (Scheme 6). Morpholinoacetic acid was first coupled to benzylalanine to provide the protected building block **28** which was then hydrogenated to yield the acid **29**.

Scheme 7 outlines the remaining construction of **11** and KZR-616 (**12**). Condensation of anisaldehyde and glycine via an Erlenmeyer condensation provided the P2 amino acid (**30**) as a racemic mixture with high diastereoselectivity which was then converted to the racemic methyl ester (**31**). Isolation of the desired enantiomer by chiral HPLC separation followed by BOC protection provided **33**. A protecting group switch to benzyl followed by BOC protection furnished the amine intermediate. The synthesis of **11** commenced with commercially available (*S*)-2-((*tert*-butoxycarbonyl)amino)-3-(4-methoxyphenyl)propanoic acid and followed the same route to completion as KZR-616 (**12**). Coupling of the P2 building block with **29** using HATU furnished the benzyl ester which was then deprotected by hydrogenation. The acid was coupled with the P1 keto-epoxide building block **26** to provide the final compounds.

Scheme 7^a

^aReagents and conditions: (i) glycine, potassium hydroxide (23%); (ii) thionyl chloride, methanol, 0 °C → rt (59%); (iii) chiral separation (45%) (iv) *tert*-butoxycarbonyl anhydride, THF (quant); (v) lithium hydroxide, methanol, THF (65%); (vi) benzyl bromide, cesium carbonate, DMF, 0 °C → rt (66%); (vii) TFA, DCM, 0 °C → rt; (viii) (2-morpholinoacetyl)-L-alanine (**29**), HATU, *N*-ethyl-*N*-isopropylpropan-2-amine (DIEA), DMF, 0 °C → rt (54% over 2 steps); (ix) hydrogen, Pd/C (10%), THF; (x) **26**, 1-[bis(dimethylamino)methylene]-1*H*-1,2,3-triazolo[4,5-*b*]pyridinium 3-oxide hexafluorophosphate (HATU), *N*-ethyl-*N*-isopropylpropan-2-amine, DMF.

Design and Evaluation. Our design of subunit selective inhibitors utilized a human homology model evolved of the murine crystal structure of the ONX 0914-proteasome isoform complexes.¹⁷ This model was developed to elucidate per subunit the optimal recognition of nonprimed selectivity pockets (S1, S2, S3) by the amino acid side chains/features (P1, P2, and P3, respectively) of epoxyketone peptidomimetic inhibitors (Figure 2a).¹⁸ Peptide epoxyketones are well-established, exquisitely chemoselective, and irreversible covalent inhibitors of N-terminal threonine proteases, a class of proteases to which the proteasomal subunits are nearly exclusive.¹⁹ We therefore chose to keep compound designs consistent with this chemical class and thus pre-engineer selectivity against other hydrolases.²⁰

We've recently reported using this homology model to design KZR-504, a highly selective peptide epoxyketone inhibitor of LMP2, which was also employed in this study.²¹ At the outset of our work, PR-924 was a known, selective inhibitor of human LMP7 (Table 1).²² Our model and recent cocrystal structures in humanized yeast proteasome²³ suggested selectivity for LMP7 arose from interactions between PR-924's indene terminus and the LMP7 S3 pocket formed at neighboring $\beta 6$. In contrast to ONX 0914 binding, a change in stereochemistry at P3 places PR-924's terminal carboxamide deep within the S3 pocket (Figure 2b). The S3 pockets of other constitutive and immunoproteasome subunits are less accommodating to either bulky or hydrophobic functionality and thus uniformly reflect lower PR-924 affinity. The epimer of PR-924, **3** (Table 1), lacks selectivity for LMP7. Modeling places its methylindene tail outside the S3 pocket and thus supports P3 stereochemistry as a driver for selectivity (Figure 2c). The use of PR-924 as a subunit selective probe in vivo was precluded by suboptimal solubility and compromised mouse LMP7/ $\beta 5$ selectivity (Table 1). Replacing the Trp-P2 substituent of PR-924 with methyltyrosine in **4** provided 2-fold

increased solubility and preserved human LMP7/ $\beta 5$ selectivity. Ala28 of the human LMP7 S3 pocket is replaced with serine in $\beta 5$ and in murine $\beta 5$ and LMP7 (Figure 2d). Ser28 constricts the S3 pocket by forming a hydrogen bond with a conserved Glu131 of the neighboring $\beta 6$ subunit. Accordingly, reducing the size of the P3 ligand from methylindene to cyclohexane (**5**) lessened human LMP7/ $\beta 5$ selectivity (Table 1, Figure 2e). However, addition of a 4-hydroxyl group to the cyclohexyl terminus in **6** increased human LMP7/ $\beta 5$ selectivity to rival that of PR-924, this while imparting >150-fold increased solubility (Table 1, Figure 2e). Like PR-924, **6** lacked selectivity for mouse LMP7. Reducing the P1-ligand size to cyclobutane in **7** resulted in significantly decreased $\beta 5$ potency, presumably through loss of optimal S1 pocket occupancy. This loss in $\beta 5$ potency translated into significantly increased mouse LMP7/ $\beta 5$ selectivity. The subtlety of this P1/mouse-S1 interaction is highlighted with **8** where replacing the P1 side chain with cyclopentenyl provided a 7-fold selectivity window for mouse LMP7 over mouse $\beta 5$. On the basis of an overall favorable in vitro profile, **8** was chosen as our LMP7 selective probe. The challenge of designing selective MECL-1 inhibitors has been highlighted elsewhere²⁴ and likely stems from a near identical substrate binding channel between MECL-1 and $\beta 2$.¹⁷ A MECL-1 inhibitor screen of our epoxyketone-peptide library brought to our attention **9** (Table 1). Like immunoproteasome selective inhibitor ONX 0914, **9** contains a solubilizing amine at its amino terminus and phenylalanine scaffolds at P1 and P2. Our modeling suggested increased MECL-1 inhibition of **9** vs ONX 0914 can be rationalized by Leu-P3 providing an optimized hydrophobic surface for interaction with Met131 of the S3 pocket (Figure 3a). Modeling ONX 0914 to MECL-1 also revealed incomplete MECL-1 S1/P1 occupancy (Figure 3b). Moreover, the S1 pocket of MECL-1 is larger and more hydrophobic than $\beta 2$ by consequence of two residue changes (T52A and D53E). With

Table 1. Subunit IC₅₀ Values and Solubility Measurements of Peptide Epoxyketones

ID	Structure	Subunit-Specific Cell Lysate IC ₅₀ (μM) ^a											Solubility (μg/mL) ^b	
		Human						Mouse						
		LMP7	β5	LMP2	β1	MECL-1	β2	LMP7	β5	LMP2	β1	MECL-1		β2
ONX-0914		0.039 ± 0.009	0.422 ± 0.090	0.287 ± 0.061	>12.7	0.902 ± 0.230	0.927 ± 0.264	0.098 ± 0.033	0.401 ± 0.095	0.328 ± 0.055	>25	0.699 ± 0.034	0.913 ± 0.082	<0.5
PR-924		0.039 ± 0.007	1.67 ± 0.507	2.21 ± 0.744	>25.0	>25.0	>25.0	0.573	1.36	4.78	N/D	N/D	N/D	0.75 ± 0.05
3		0.038	0.054	N/D	N/D	N/D	N/D	0.05	0.047	N/D	N/D	N/D	N/D	1.85 ± 0.05
4		0.076 ± 0.001	3.62 ± 1.30	N/D	N/D	N/D	N/D	0.764 ± 0.001	2.34 ± 1.08	N/D	N/D	N/D	N/D	1.40 ± 0.20
5		0.029	0.185	N/D	N/D	N/D	N/D	0.141	0.118	N/D	N/D	N/D	N/D	12.1 ± 3.5
6		0.023 ± 0.002	0.782 ± 0.243	3.53	>25.0	>25.0	>25.0	0.262 ± 0.025	0.507 ± 0.009	N/D	N/D	N/D	N/D	240.0 ± 2.8
7		0.262	6.63	N/D	N/D	N/D	N/D	0.556	6.81	N/D	N/D	N/D	N/D	979.1 ± 15.1
8		0.034 ± 0.001	2.67 ± 0.277	1.85 ± 0.169	>25.0	>25.0	>25.0	0.374 ± 0.017	2.65 ± 0.587	3.96	N/D	N/D	N/D	491.3 ± 0.7
9		0.049	0.039	0.415	>250	0.097 ± 0.025	0.081 ± 0.013	0.056	0.038	0.415	>250	0.159	0.141	nd
10		0.346 ± 0.008	0.486 ± 0.068	>25.0	>25.0	0.071 ± 0.053	0.413 ± 0.115	1.92 ± 0.214	0.378 ± 0.009	>25.0	>25.0	0.305 ± 0.041	0.573 ± 0.102	7.0 ± 0.4
11		0.083 ± 0.015	0.926 ± 0.160	0.223	36.421	1.437	1.176	0.110 ± 0.014	0.694 ± 0.066	N/D	N/D	N/D	N/D	2730.8 ± 151.6
KZR-616 (12)		0.039 ± 0.005	0.688 ± 0.160	0.131 ± 0.013	>10.6	0.623 ± 0.040	0.604 ± 0.044	0.057 ± 0.018	0.483 ± 0.092	0.179 ± 0.003	>25	0.522	0.857	7072.1 ± 518.8

^aBy utilization of MOLT-4 (human T cell leukemia) or A20 (mouse B-cell lymphoma) cellular lysate, a proteasome constitutive/immunoproteasome subunit ELISA (ProCISE) was employed for quantitative assessment of subunit-specific activity. Data are reported as the mean ± SD ($n \geq 2$).

10, increased size and reach of the hydrophobic P1 substituent provided improvements to MECL-1 inhibition and selectivity

over β2 (Table 1). Although proteasome active site subunits bear distinguishing features outside the S1 pocket, it is largely

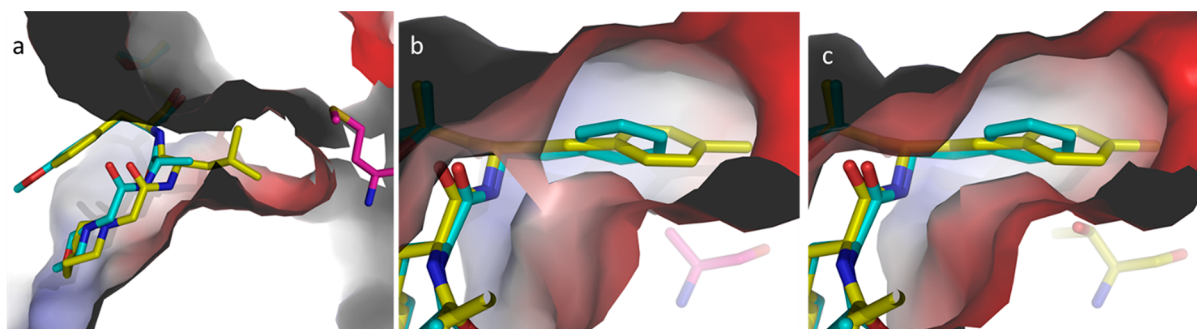


Figure 3. Modeling of ONX 0914 in blue and **10** in yellow. (a) van der Waals surfaces depicted with a cutaway of the S3 pocket. Met131 is depicted in magenta. (b) van der Waals surfaces depicted with a cutaway of the S1 pocket. (c) Human MECL-1. In the binding site, there is only a single residue difference (A52T) from human to mouse. Ala52 is depicted in magenta.

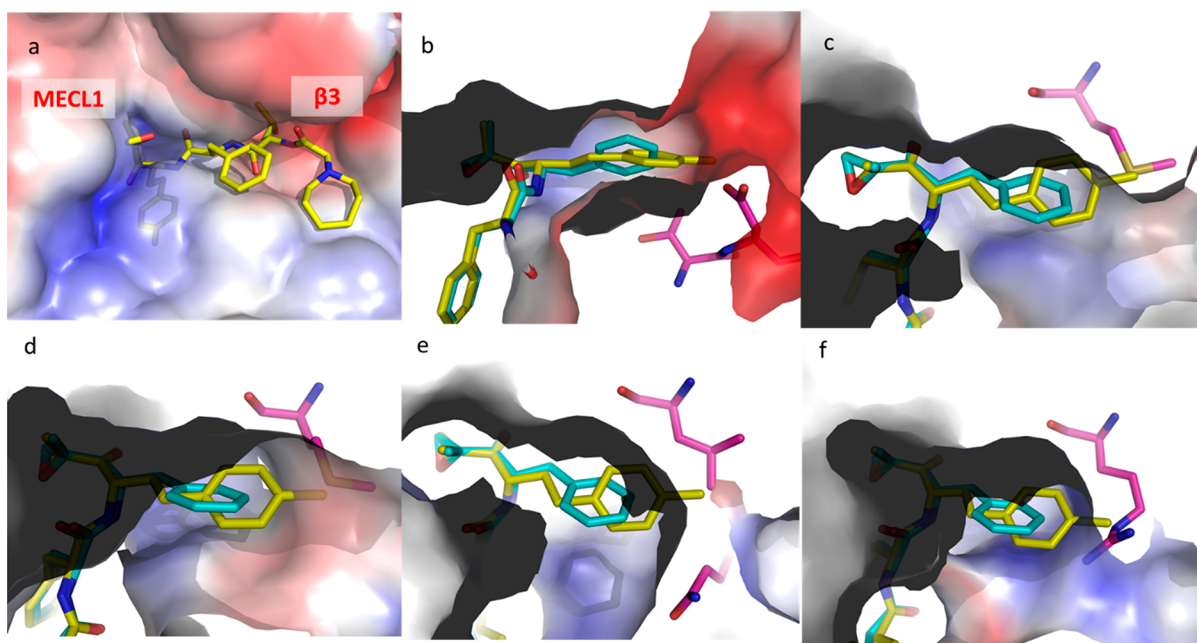


Figure 4. Modeling of **10** within proteasome catalytic binding sites. van der Waals surfaces are depicted with **10** in yellow, and for comparison, ONX 0914 is in blue. (a) **10** modeled with human MECL-1. (b) Cutaway of the S1 pocket of the human $\beta 2$ binding site with **10** and ONX 0914 overlaid. Key residues distinguishing $\beta 2$ from MECL-1, Thr52, and Asp53 are depicted in magenta. (c) Cutaway of the S1 pocket of the human LMP7 binding site with **10** and ONX 0914 overlaid. Met45 is depicted in magenta. A steric clash between Met45 and the P1 substituent of **10** prevents this ligand from binding efficiently to LMP7. (d) Cutaway of the S1 pocket of the human $\beta 5$ binding site with **10** and ONX 0914 overlaid. Met45 is depicted in magenta. Like LMP7, a steric clash between Met45 and the P1 substituent of **10** prevents this ligand from binding efficiently to $\beta 5$. (e) Cutaway of the S1 pocket of the human $\beta 5$ binding site with **10** and ONX 0914 overlaid. Residues different from MECL-1 are depicted in magenta: G45L and E53Q; C31F is not shown for clarity. The LMP2 pocket is shallower than MECL-1. (f) Cutaway of the S1 pocket of the human $\beta 1$ binding site with **10** and ONX 0914 overlaid. A key residue difference from MECL-1 is a glycine to arginine switch at position 45 (shown in magenta), making the $\beta 1$ pocket significantly shallower than MECL-1.

differences within this pocket which drive selective inhibition of human MECL-1 by **10** (Figure 4). However, designing a cross-species selective MECL-1 inhibitor was problematic. Going from human to mouse, alanine at position 52 is replaced by a threonine which creates a smaller, more polar S1 pocket in mouse MECL-1 relative to the human ortholog (Figure 3c). Relative to human, this difference triggered 4-fold reduced mouse MECL-1 inhibition and precluded advancement of **10** to our disease model. Further efforts to rescue mouse MECL-1 potency within the **10** chemotype proved challenging.

Human leukemia cells (MOLT-4) expressing both forms of the proteasome were used to determine full subunit-selective inhibitory concentrations of ONX 0914, **8**, **10**, and KZR-504 using proteasome constitutive/immunoproteasome subunit

ELISA (ProCISE)^{22,25} (Supporting Information Figure 1). From these data, we chose individual concentrations to test in peripheral blood mononuclear cells (PBMC), which express essentially only the immunoproteasome. We found that that immunoproteasome subunit inhibition in human PBMC reflected MOLT-4 inhibition upon individual and combination compound exposure (Figure 5a, Figure 5b). This enabled assessment of inflammatory cytokine expression in LPS stimulated and anti-CD3/CD28 stimulated PBMC upon discrete and combined subunit inhibition (Figure 5a, Figure 5b).

Consistent with previous reports,^{13,16,26} ONX 0914 potently reduced cytokine expression in stimulated PBMC (Figure 5a). By comparison, selective LMP7 inhibition by **8** in LPS

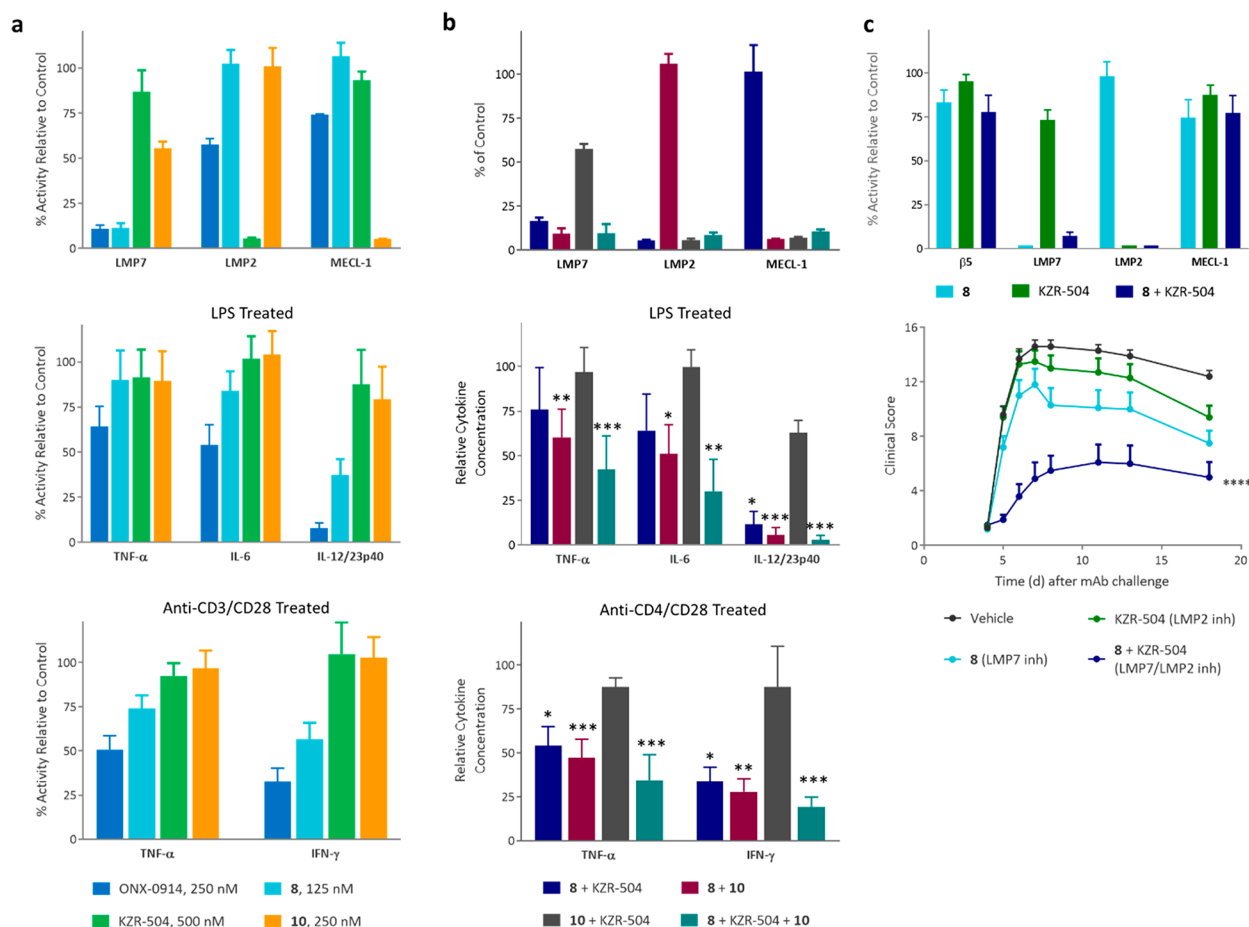


Figure 5. Effect of LMP7, LMP2, and MECL-1 selective subunit inhibitors alone and in combination. Active site occupancy was measured using ProCISE, and activity (probe occupancy) for LMP7, LMP2, and MECL-1 subunits was normalized to DMSO-treated controls. PBMC were treated with either 250 nM ONX 0914, 125 nM **8**, 500 nM KZR-504, 250 nM **10** alone (a) or in combination (b) for 1 h and then stimulated with 1 $\mu\text{g}/\text{mL}$ LPS or antibodies against CD3 and CD28 for 24 h. Supernatants were analyzed for TNF α , IL-6, the p40 subunit of IL-12/23, and IFN γ via electrochemiluminescent ELISA (Meso Scale Discovery). Data are presented as mean relative level \pm SD ($n = 6$) compared to DMSO-treated controls: * = $P < 0.05$; ** = $P < 0.01$; *** = $P < 0.001$ vs DMSO controls by Friedman test followed by Dunn's posthoc comparison of absolute cytokine levels. (c) BALB/c mice were coadministered (iv) **8** at 20 mg/kg and KZR-504 at 5 mg/kg and in combination. Kidney and splenocyte (erythrocyte-depleted) samples were taken 1 h after dosing, and the activity of LMP7, LMP2, MECL-1 (splenocytes), and $\beta 5$ (kidney) was measured by ProCISE. Data were normalized to the average activity of vehicle-treated animals and are presented as the average relative activity \pm SD ($n = 3$). BALB/c mice received 1.75 mg of a cocktail of five antibodies against type II collagen on day 0 followed by 25 μg of LPS on day 3. On day 4, when disease symptoms were present in all mice, animals were randomized into four groups and were treated iv with vehicle, **8** at 20 mg/kg, KZR-504 at 5 mg/kg, or the combination of **8** at 20 mg/kg and KZR-504 at 5 mg/kg. Dosing was repeated on days 6, 8, 11, 13, and 15, and clinical scores (0–4/paw; $n = 7/\text{group}$) were followed until day 18. Data, presented as the mean clinical score \pm SEM, are from one experiment of two performed with similar results: **** = $P < 0.0001$ by two-way ANOVA followed by Bonferroni post hoc comparison at the end of study.

stimulated PBMC failed to significantly reduce TNF α and IL-6 and only partially inhibited the p40 subunit of IL-12/23. TNF α and IFN- γ expression in anti-CD3/CD28 stimulated PBMC was inhibited by **8** but significantly less so than by ONX0914 treatment. Neither KZR-504 nor **10** significantly reduced cytokine expression in LPS or anti-CD3/CD28 stimulated cells. When either KZR-504 or **10** was combined with **8**, the cytokine inhibition profile matched that of ONX 0914 (Figure 5b). However, the combination of KZR-504 and **10** did not result in significant inhibition of cytokine secretion under either stimulation condition. These data indicate that LMP7 inhibition is necessary but not sufficient for the full cytokine inhibition profile of ONX 0914. Inhibition of all three subunits of the immunoproteasome, achieved with the combination of **8**, KZR-504, and **10**, resulted in the greatest effect on cytokine secretion, though a 30% reduction in cell viability was noted (data not shown).

ONX 0914 mediates anti-inflammatory responses in mouse models of rheumatoid arthritis at doses resulting in inhibition of multiple immunoproteasome subunits.¹³ Peptide epoxyketones show rapid pharmacokinetic clearance across species (typical half-life $t_{1/2} < 15$ min),²⁷ yet like other covalent inhibitors, their pharmacodynamic effects outlast compound pharmacokinetics and reflect turnover of covalently inhibited enzyme in pervaded tissues.²⁸ Pharmacokinetics of compounds **8** and KZR-504 upon intravenous administration to BALB/c mice are also comparably rapid ($t_{1/2} < 7$ min, clearance of >73 mL min^{-1} kg^{-1} , Supporting Information Table 1). To test the pharmacodynamic effect of individual and combined subunit inhibition in vivo, **8**, KZR-504, or their combination was administered to BALB/c mice, and subunit inhibition profiles in tissues (spleen and kidney) were evaluated at 1 h, a time point easily capturing exposure and clearance for both compounds. Subunit selective inhibitory doses were estab-

lished for **8** and KZR-504 at 5 and 20 mg/kg, respectively. Like in vitro results in human PBMC, subunit inhibition profiles in combination reflected the individual compound administration effects (Figure 5c). Next, subunit selective inhibitory doses were used to explore the therapeutic effect of individual and combined subunit inhibition in mice with active collagen antibody induced arthritis. Single agent treatment of diseased mice with KZR-504 and **8** had a negligible impact on disease progression, indicating that individual subunit inhibition is insufficient to inhibit inflammation in vivo. In contrast, the combination treatment with KZR-504 and **8** resulted in significant reduction of disease burden to levels similar to that of ONX 0914 treatment alone. On the basis of body weights and cage-side observations, we did not detect a change in tolerability between any treatment group (data not shown). Although ONX 0914 possesses an efficacious immunoproteasome subunit inhibition repertoire, its suboptimal solubility precluded further clinical development (Table 1). Upon replacement of the planar, hydrophobic P1 phenylalanine side chain with saturated or semisaturated ring systems, unformulated solubility improvements were observed among the cyclohexanol bearing compounds (**6** vs **7** and **8**, Table 1). Among these compounds, the P1 cyclopentene of KZR 329 offered improved solubility and optimal LMP7 selectivity. Incorporation of this feature into the ONX 0914 scaffold resulted in a desired subunit inhibition profile with vastly improved solubility (**11**). Toward furthering solubility, our modeling indicated that an *R*-hydroxyl group substitution at the β position of the P2 methyltyrosine side chain would be well tolerated and result in hydrogen-bonding with Ser21. Merging of these features provided KZR-616 (**12**, Figure 6), a

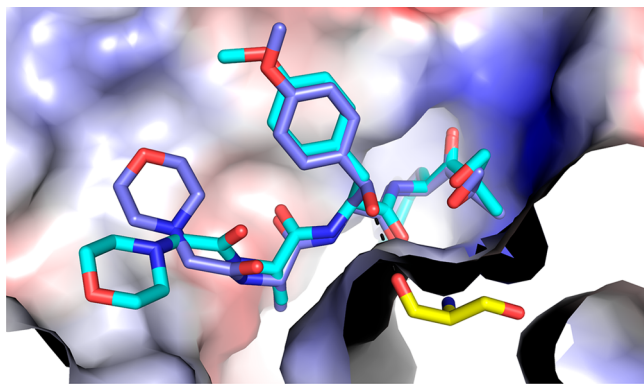


Figure 6. Modeling of KZR-616 in the LMP7/ β 6 binding site. Similar binding modes are observed for ONX 0914 (blue) and KZR-616 (purple). van der Waals surfaces are shown. A productive H-bonding interaction takes place between KZR-616 and backbone carbonyl of Ser21 (yellow). An increase in binding affinity and solubility is realized with the addition of the P2 alcohol functionality.

compound with 2.5-fold improved solubility relative to **11**. Relative to ONX 0914, KZR-616 maintained LMP7 and LMP2 selective inhibition (Figure 7a), a comparable cytokine inhibition profile (Figure 7a, Figure 7b), and similar rapid pharmacokinetics (Supporting Information Table 1). Moreover, efficacy of KZR-616 was comparable to ONX 0914 in the anticollagen antibody induced arthritis (CAIA) model at half the dosage (Figure 7b) while subcutaneous administration gave comparable results at similar dosages (data not shown). As expected of compounds from the epoxyketone chemical class, KZR-616 showed no inhibition at 10 μ M against a broad

selectivity panel of 20 serine, metallo-, cysteine, and aspartyl proteases and 11 hydrolases (Supporting Information Table 2 and screening panel methods). Based in part on these results, KZR-616 was selected as a clinical candidate for treatment of autoimmune disease.

CONCLUSION

This is the first study to describe and employ a library of immunoproteasome subunit-specific inhibitors to probe the role of individual subunits in regulation of cytokine secretion and inflammation. These results demonstrate that while necessary, inhibition of LMP7 alone was insufficient to inhibit cytokine expression in activated immune effector cells or prevent disease progression in a mouse model of autoimmunity. Thus, previously published effects of ONX 0914 likely reflect the combined inhibition of multiple immunoproteasome subunits. To demonstrate this, we see that a combination of LMP7 and MECL-1 and/or LMP2 inhibitors offered an optimal cytokine inhibition profile in vitro, which, in the case of dual LMP7 and LMP2 inhibition, was predictive of efficacy in a mouse model of inflammatory arthritis. In PBMC exposed to fully inhibitory concentrations of all three subunit-selective inhibitors, greater cytokine inhibition was achieved relative to ONX 0914 but was also associated with a loss of viability in the cells (data not shown). It is noteworthy that dual inhibitors KZR-616 and ONX 0914 achieved activity in the mouse arthritis model via complete LMP7 inhibition and \sim 40% LMP2 inhibition, suggesting that only partial inhibition of a secondary immunoproteasome subunit is required for a multicytokine inhibitory effect. In addition to providing further clarity for the necessary immunoproteasome subunit inhibition profile for treatment of autoimmune disorders, these findings and discoveries toward improved physicochemical properties have been applied to our clinical candidate KZR-616, now in clinical trials for treatment of rheumatic diseases.²⁹

EXPERIMENTAL SECTION

General Procedures. Cells. MOLT-4 (human T-cell leukemia) and A20 (mouse B-cell lymphoma) cell lines (ATCC, Manassas, VA) were cultured in RPMI 1640 media (with 300 mg/L L-glutamine) supplemented with 10% heat-inactivated fetal bovine serum (FBS), 0.15% (w/v) sodium bicarbonate, 0.45% (w/v) glucose, 10 mM HEPES, 1 mM sodium pyruvate, 100 IU penicillin, and 100 μ g/mL streptomycin (Corning Mediatech, Manassas, VA). A20 medium was also supplemented with 0.05 mM β -mercaptoethanol (Sigma-Aldrich, St. Louis, MO). Cryopreserved peripheral blood mononuclear cells (PBMCs) from normal healthy volunteers were purchased from AllCells (Alameda, CA) and cultured in RPMI 1640 media (with 300 mg/L L-glutamine) supplemented with 5% heat-inactivated FBS, 100 IU penicillin, and 100 μ g/mL streptomycin (Corning Mediatech, Manassas, VA). Cellular lysate was generated by 15–30 min incubation of freeze–thawed cell pellets on ice, twice in the pellet volume of hypotonic lysis buffer (20 mM Tris, pH 8, 5 mM EDTA), with occasional vortexing. Uncleared lysate was then centrifuged at 4 $^{\circ}$ C at 18 000g to 18 500g for 15 min, and the supernatant (cleared lysate) was collected for protein quantitation via bicinchoninic acid (BCA) assay (Thermo Scientific Pierce, Rockford, IL) against a bovine serum albumin (BSA) standard curve and subsequent proteasome activity analysis. Lysate was kept on ice during all subsequent handling or stored between analyses at -80 $^{\circ}$ C.

Proteasome Active Site ELISA (ProCISE).²² An enzyme-linked immunosorbent assay (ELISA)-based technique, the proteasome constitutive/immunoproteasome subunit ELISA (ProCISE) assay, was utilized for quantitative assessment of subunit-specific activity as previously described.¹ For cell lysate analysis, test compounds were

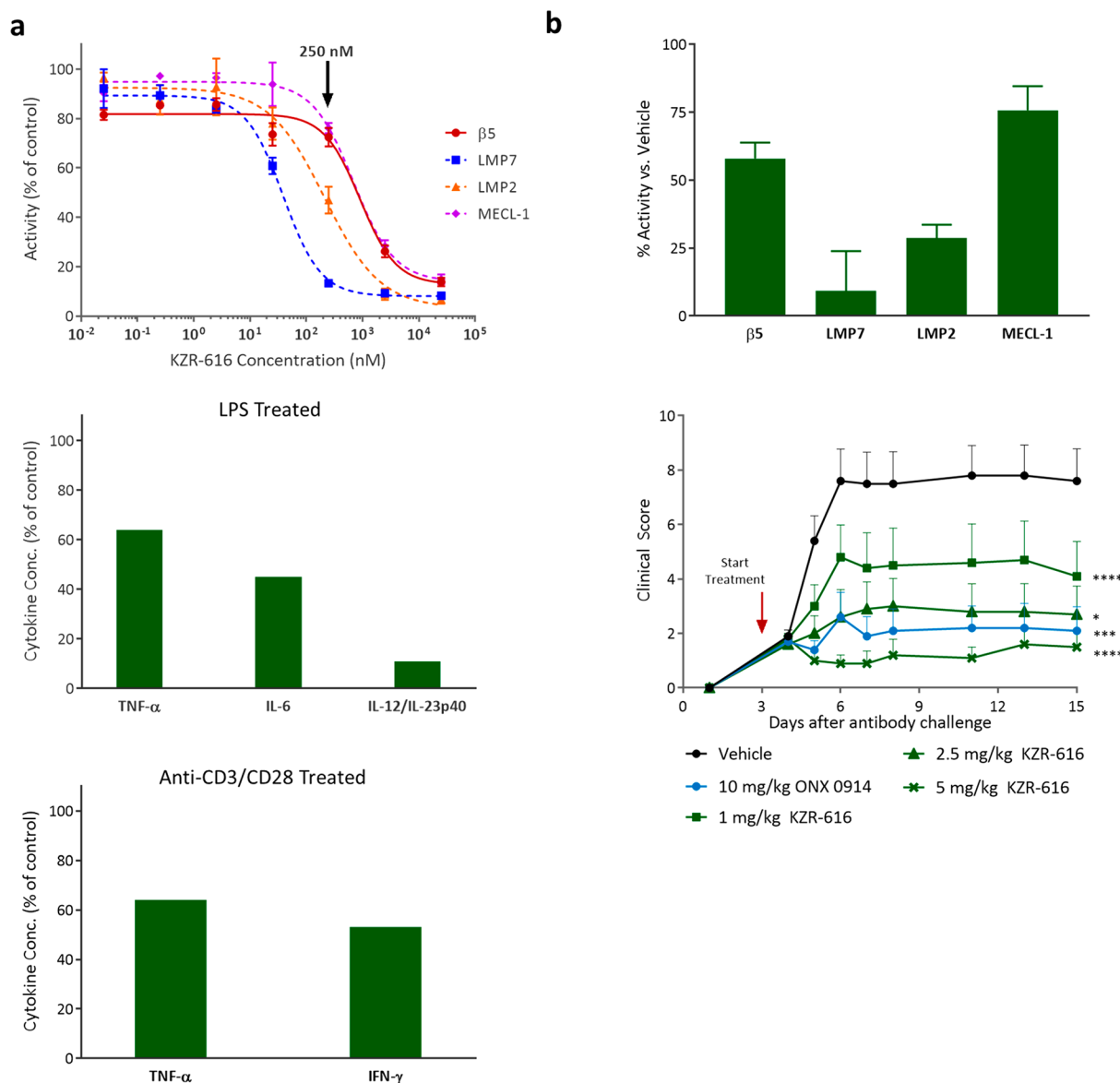


Figure 7. Effect of KZR-616. (a) Active site ELISA analysis of MOLT-4 cells following proteasome inhibition with KZR-616 and corresponding cytokine inhibition in stimulated PBMC at selective concentration (250 nM). (b) Top panel: BALB/c mice were administered (iv) KZR-616 at 5 mg/kg. Kidney and splenocyte (erythrocyte-depleted) samples were taken 1 h after dosing, and the activity of LMP7, LMP2, MECL-1 (splenocytes), and $\beta 5$ (kidney) was measured by ProCISE. Data were normalized to the average activity of vehicle-treated animals and are presented as the average relative activity \pm SD ($n = 3$). Lower panel: BALB/c mice received 1.75 mg of a cocktail of five antibodies against type II collagen on day 0 followed by 25 μ g of LPS on day 3. On day 4, when disease symptoms were present in all mice, animals were randomized into five groups and were treated iv with vehicle, KZR-616, or ONX 0914 at dosages shown. Dosing was repeated on days 6, 8, 11, and 13, and clinical scores (0–4/paw; $n = 7$ /group) were followed until day 15. Data, presented as the mean clinical score \pm SEM, are from one experiment of two performed with similar results: * = $P < 0.0133$, *** = $P < 0.001$, **** = $P < 0.0001$ by two-way ANOVA followed by Bonferroni post hoc comparison at the end of study.

serially diluted in DMSO at 100 \times concentration, then diluted to 10 \times in hypotonic lysis buffer (20 mM Tris, pH 8, 5 mM EDTA). MOLT-4 or A20 cell lysate was treated for 1 h at 25 $^{\circ}$ C with compound at a final 1 \times concentration (1 mg/mL final lysate concentration). For MOLT-4 whole (live) cell analysis, compounds were serially diluted in DMSO at 400 \times concentration, then diluted to 5 \times in cell growth media. Compounds were added to live MOLT-4 cells suspended at \sim 2 million cells/mL and incubated for 1 h at 37 $^{\circ}$ C, 5% CO $_2$ at a final 1 \times concentration. Whole cells were then washed 3 times in phosphate buffered saline (PBS), frozen at -80 $^{\circ}$ C, thawed, and processed to lysate. For PBMC whole (live) cell analysis, compounds were diluted in DMSO at 2000 \times concentration, then diluted to 2 \times in cell growth media. Compounds were added to live PBMCs suspended at 1 million

cells/mL and incubated for 1 h at 37 $^{\circ}$ C, 5% CO $_2$ at a final 1 \times concentration. Whole cells were then washed 4 times in phosphate buffered saline (PBS), frozen at -80 $^{\circ}$ C, thawed, and processed to lysate. Treated cell lysate (1 mg/mL) was incubated with a biotinylated proteasome active site binding probe (Nanosyn, Santa Clara, CA; 5 μ M final) for 2 h at 25 $^{\circ}$ C. Following this, lysate (0.1 mg/mL final) was denatured in guanidine hydrochloride (Sigma-Aldrich, St. Louis, MO; 5.6 M final), and subunits bound to probe were isolated with streptavidin-conjugated sepharose beads (GE Healthcare Bio-Sciences, Uppsala, Sweden; 1:20 dilution of original stock volume) via 1 h incubation in 0.65 μ m filter plates (EMD Millipore, Billerica, MA) at 25 $^{\circ}$ C with vigorous shaking. Multiple rinses in wash buffer (1 \times PBS, 0.1% Tween 20, 1% BSA; Teknova,

Hollister, CA) were utilized to remove denaturant, and individual subunits were probed overnight at 4 °C (with shaking) with subunit-specific primary antibodies (Covance, Denver, PA; Enzo Life Sciences, Farmingdale, NY; Santa Cruz Biotechnology, Santa Cruz, CA). Following primary antibody removal and washing, samples were incubated for 2 h with HRP-conjugated secondary antibodies (Jackson ImmunoResearch, West Grove, PA; Invitrogen, Carlsbad, CA). Finally, secondary antibody was eliminated and a chemiluminescent substrate (Thermo Scientific Pierce, Rockford, IL) was used to generate signal associated with HRP binding, which was detected on a plate reader (Tecan, Männedorf, Switzerland). Luminescent signal was normalized to protein content and then percent activity calculated relative to DMSO-treated controls to generate IC₅₀ curves.

PBMC Stimulation and Cytokine Analysis. PBMCs (250 000 cells/well) were plated in culture media in 96-well round-bottom plates (Corning, Corning, NY). An equal volume of compounds diluted in media were then added (final DMSO concentration of 0.1%). After 1 h incubation at 37 °C, 5% CO₂, plates were washed 4 times with culture media. Following compound washout, PBMCs were stimulated with either lipopolysaccharide (LPS, *Escherichia coli*, O111:B4, EMD Millipore, Billerica, MA) at 1 µg/mL or antibodies to CD3 (coated overnight at 2 µg/mL in PBS and then washed out, OKT3, Thermo Fisher Scientific, San Diego, CA) and CD28 (2 µg/mL in media, BD Biosciences, San Jose, CA) for 24 h. Supernatants were then collected and analyzed for TNFα, IL-6, IL-12/23p40, and IFNγ by Meso Scale Discovery electrochemiluminescent immunoassay detection (MSD).

Mice. BALB/c mice (H-2^d) were purchased from Taconic Labs. All experiments were done under protocols approved by an institutional animal care and use committee.

Arthritis Model. Anti-collagen antibody induced arthritis (CAIA) was induced in 7–8 week old female BALB/c mice (kept on breeder chow) by an intravenous (iv) administration of 1.75 mg of a cocktail of 5 antibodies against type II collagen (Chondrex, Redmond, WA) followed by intraperitoneal challenge with 25 µg LPS on day 3. Treatment was initiated after clinical signs of arthritis were observed (day 4). Paws were scored for disease severity on a 0 (no disease) to 4 (maximal swelling) scoring system and summed for individual animal scores. For ANOVA, Bonferroni post hoc analysis was used to compare treatment groups. All statistical analyses were performed using GraphPad Prism software (version 7.01, La Jolla, CA). Statistical significance was achieved when *P* was less than 0.05. 8, KZR-504, 10, and ONX 0914 were all formulated in an aqueous solution of 10% (w/v) sulfobutyl ether-β-cyclodextrin and 10 mM sodium citrate (pH 3.5) and administered to mice as a single iv bolus. For proteasome activity determination, whole blood (sodium heparin anti-coagulant) and tissue samples (kidney and spleen) were collected 1 h after administration and processed as described below for protein quantitation and ProCISE analysis.

Mouse Tissue Pharmacodynamics. Following collection 1 h after compound administration, an amount of ~500 µL of whole blood samples was washed 3 times in 5 mL of PBS, and the resultant blood pellet was frozen at –80 °C. Kidney was immediately frozen on dry ice and stored at –80 °C. Spleen was passed through a 100 µm cell strainer, underwent red blood cell lysis (Pharm Lyse, BD Biosciences, San Jose, CA), and was rinsed in PBS before freezing of the splenocyte pellet at –80 °C. Frozen tissue samples were later thawed on ice in preparation for lysate collection. Hypotonic lysis buffer (20 mM Tris, pH 8, 5 mM EDTA; approximately twice the volume of cell pellet/tissue) was added to each sample. Whole blood and splenocyte pellets were lysed for 15–30 min on ice, with occasional vortexing. A 5 mm stainless steel bead (QIAGEN, Hilden, Germany) was added to each kidney sample in a 2 mL micro-centrifuge tube. Solid tissue was bead-homogenized on a TissueLyser (QIAGEN, Hilden, Germany) for 2 min at 20 Hz. All pellet and tissue samples were then centrifuged at 18 000g to 18 500g at 4 °C for 15 min. Supernatant (lysate) was collected and kept on ice during subsequent handling. Tissue lysate was diluted in lysis buffer for protein quantification via BCA assay (Thermo Scientific Pierce, Rockford, IL) against a BSA standard curve. Following determination

of protein concentration, lysate was diluted to appropriate concentrations for ProCISE probe binding and plate loading: 10 mg/mL (blood), 5 mg/mL (kidney), and 1 mg/mL (spleen). Inhibition of subunit-specific proteasome active sites was quantified utilizing the ProCISE assay as described above. Luminescent signal was normalized to protein content, and protein-normalized background signal from DMSO-probed control samples was subtracted. Percent activity was then calculated relative to vehicle-treated animals.

Mouse Pharmacokinetics. Pharmacokinetics of 8, KZR-504, KZR-616, and ONX 0914 were evaluated in 7–8 week old female BALB/c (Charles Rivers Laboratory) mice administered at 2 mg/kg each intravenously in a vehicle of 25% PEG300/WFI. Mice were euthanized (CO₂ narcosis) at 2, 5, 10, 20, 30, 60, and 120 min postdose. Blood was collected via cardiac puncture in sodium heparin containing tubes and processed to plasma (*n* = 3/time point). Acetonitrile was used to precipitate plasma proteins, and drug concentrations were determined by LC–MS/MS. Noncompartmental analysis was applied to the mean plasma concentrations at each time point. Nominal times and target doses were used in PK analysis. Reported pharmacodynamic parameters were determined by fit using Phoenix WinNonlin (version 6.4, Pharsight Inc., S. Louis, MO).

Generation of Homology Models. Protein homology models were generated for the active sites of human subunits based on the mouse crystal structures, PDB code 3UNB. The human sequences were aligned to the appropriate mouse structural subunits, structures were cleaned and parametrized with the AMBER12/EHT force field, and a homology model was built following standard protocols in MOE 2013.08 from Chemical Computing Group (Molecular Operating Environment, 2013.08; Chemical Computing Group Inc., 1010 Sherbooke Street West, Suite No. 910, Montreal, QC, Canada, H3A 2R7, 2015).

Generation of Ligand Binding Models. Starting ligand structures were imported as SMILES into MOE 2013.08 using standard protocols for Wash, Parameterization, and low mode 3D conformer search with the AMBER12/EHT force field in MOE 2013.08. Ligands were modeled within the active sites using a two-step process. First they were aligned to crystal ligand (ONX 0914) conformer position in the appropriate proteasome subsite from the 3UNB structure using standard MOE process for rigid and flexible alignment. The initial poses were optimized in homology model binding site using MOE LigX in-site minimization, where protein atoms >10 Å from ligands were fixed and inert, protein atoms >8 Å were fixed, protein site <8 Å was subject to 20 kcal/0.5 Å tether, and the ligand was completely free to move. Figures were created using Pymol version 1.5.0.4. (The PyMol Molecular Graphics System, version 1.5.0.4, Schrodinger, LLC.)

Peptidase/Hydrolase Panel. Results were part of a broad Cerep Panlabs selectivity panel against KZR-616 maleate salt (10 µM) performed in replicate at Eurofins Panlabs Tawain, Ltd. Methods of the 31 assays are detailed in [Supporting Information](#).

Chemical Synthesis. General Procedures of Chemical Synthesis. All reagents and solvents employed were purchased commercially and used without further purification unless otherwise indicated. All tested compounds were >95% pure as assayed by analytical HPLC using an Agilent 1260 Infinity system with an Atlantis T3 150 mm × 4.6 mm column at a 1.0 mL/min flow rate with a gradient of 0–95% acetonitrile/water (both solvents containing 0.1% aqueous TFA) for 20 min. ¹H NMR spectra were recorded on either a JEOL ECX (400 MHz) or a Bruker AVANCE III (400 MHz) spectrometer. Chemical shifts are provided in ppm (δ) relative to DMSO-*d*₆ or CDCl₃ as an internal standard. LC–MS analysis was performed on an Agilent 6120 Single Quad MS with a 1260 Infinity HPLC and EclipsePlus C18, 2.1 mm × 50 mm column at a 0.3 mL/min flow rate with a gradient of 0–95% acetonitrile/water (both solvents containing 0.1% aqueous TFA) for 3 min. Flash column chromatography was carried out using an ISCO Combiflash Rf-200 system with a 200–360 variable wavelength detector and a gradient of 0–10% methanol in dichloromethane/ethyl acetate (3:1) unless otherwise noted. Syntheses of peptide epoxyketones in this work and related art have also been published elsewhere.³⁰ PR-924 (IPSI) is

published elsewhere.³¹ (S)-2-Amino-1-((R)-2-methyloxiran-2-yl)-3-phenylpropan-1-one TFA salt is published elsewhere.³²

N-((S)-1-(((S)-3-(1H-Indol-3-yl)-1-((S)-1-((R)-2-methyloxiran-2-yl)-1-oxo-3-phenylpropan-2-yl)amino)-1-oxopropan-2-yl)amino)-1-oxopropan-2-yl)-3-methyl-1H-indene-2-carboxamide (3). The title compound was prepared in analogy to 4. ¹H NMR (400 MHz, CDCl₃) δ 7.97–7.89 (s, 1H), 7.67–7.58 (m, 1H), 7.45 (m, 2H), 7.41–7.31 (m, 2H), 7.24–7.18 (m, 1H), 7.19–7.04 (m, 5H), 6.92 (d, J = 2.4 Hz, 1H), 6.89–6.82 (m, 2H), 6.72 (d, J = 7.6 Hz, 1H), 6.31 (d, J = 7.6 Hz, 1H), 6.08 (d, J = 6.8 Hz, 1H), 4.70 (m, 2H), 4.55 (m, 1H), 3.40 (dd, J = 22.2, 2.4 Hz, 1H), 3.35–3.26 (m, 2H), 3.26–3.17 (m, 1H), 3.07 (dd, J = 14.6, 7.4 Hz, 1H), 2.99 (dd, J = 13.9, 4.9 Hz, 1H), 2.85 (d, J = 4.9 Hz, 1H), 2.60 (dd, J = 13.9, 8.2 Hz, 1H), 2.45 (t, J = 2.3 Hz, 3H), 1.45 (s, 3H), 1.39 (d, J = 7.0 Hz, 3H); ¹³C NMR (125 MHz, CDCl₃): δ 207.1, 172.3, 170.8, 166.0, 148.2, 145.4, 142.1, 136.1, 135.8, 131.2, 129.2, 128.4, 127.4, 127.3, 126.9, 126.8, 123.8, 123.6, 122.2, 120.9, 119.7, 118.6, 111.3, 109.9, 59.1, 53.6, 52.6, 52.4, 49.0, 38.0, 37.0, 27.6, 18.3, 16.4, 12.3. HRMS (m/z): [M]⁺ calcd for C₃₇H₃₉N₄O₅, 619.2920; found, 619.2934.

N-((R)-1-(((S)-3-(4-Methoxyphenyl)-1-((S)-1-((R)-2-methyloxiran-2-yl)-1-oxo-3-phenylpropan-2-yl)amino)-1-oxopropan-2-yl)amino)-1-oxopropan-2-yl)-3-methyl-1H-indene-2-carboxamide (4). To (S)-2-((tert-butoxycarbonyl)amino)-3-(4-methoxyphenyl)propanoic acid (10.0 g, 33.9 mmol) in DMF (10 mL) at 0 °C were added HOBT (4.81 g, 37.3 mmol) and HBTU (14.1 g, 37.3 mmol). The mixture was stirred for 5 min to dissolve solids, at which time (S)-2-amino-1-((R)-2-methyloxiran-2-yl)-3-phenylpropan-1-one TFA salt (10.2 g, 33.9 mmol) and DIEA (17.4 mL, 0.101 mol) were added. The reaction mixture was stirred at ambient temperature for 30 min and then quenched with sodium bicarbonate (sat.), extracted with ethyl acetate (2×), dried with sodium sulfate, filtered, and concentrated. Purification by column chromatography (0–60% ethyl acetate/heptane) provided tert-butyl ((S)-3-(4-methoxyphenyl)-1-(((S)-1-((R)-2-methyloxiran-2-yl)-1-oxo-3-phenylpropan-2-yl)amino)-1-oxopropan-2-yl)carbamate (13.4 g, 82%) as a colorless amorphous solid. MS (EI) for C₂₇H₃₄N₂O₆, found 483.3 (MH⁺).

To tert-butyl ((S)-3-(4-methoxyphenyl)-1-(((S)-1-((R)-2-methyloxiran-2-yl)-1-oxo-3-phenylpropan-2-yl)amino)-1-oxopropan-2-yl)carbamate (1.00 g, 2.07 mmol) were added DCM (5 mL) and TFA (5 mL). The reaction mixture was stirred for 15 min at ambient temperature and then concentrated and carried forward without further purification. (S)-2-Amino-3-(4-methoxyphenyl)-N-((S)-1-((R)-2-methyloxiran-2-yl)-1-oxo-3-phenylpropan-2-yl)propanamide TFA salt was immediately carried forward into the subsequent step (quant yield). MS (EI) for C₂₂H₂₆N₂O₄, found 383.2 (MH⁺).

To (S)-2-amino-3-(4-methoxyphenyl)-N-((S)-1-((R)-2-methyloxiran-2-yl)-1-oxo-3-phenylpropan-2-yl)propanamide TFA salt (2.07 mmol) were added (R)-2-((tert-butoxycarbonyl)amino)propanoic acid (782 mg, 4.14 mmol), HATU (1.82 g, 4.77 mmol), and DMF (7 mL). The mixture was cooled to 0 °C, and DIEA (3.54 mL, 20.7 mmol) was added. The reaction mixture was stirred at ambient temperature for 30 min and then quenched with sodium bicarbonate (sat.), extracted with ethyl acetate (2×), dried with sodium sulfate, filtered, and concentrated. Purification by column chromatography (0–80% ethyl acetate/heptane) provided tert-butyl ((S)-1-(((S)-3-(4-methoxyphenyl)-1-(((S)-1-((R)-2-methyloxiran-2-yl)-1-oxo-3-phenylpropan-2-yl)amino)-1-oxopropan-2-yl)amino)-1-oxopropan-2-yl)carbamate (897 mg, 89%) as a colorless solid. MS (EI) for C₂₆H₃₇N₃O₆, found 488.4 (MH⁺).

To tert-butyl ((S)-1-(((S)-3-(4-methoxyphenyl)-1-(((S)-1-((R)-2-methyloxiran-2-yl)-1-oxo-3-phenylpropan-2-yl)amino)-1-oxopropan-2-yl)amino)-1-oxopropan-2-yl)carbamate (190 mg, 0.412 mmol) were added DCM (2 mL) and TFA (2 mL). The reaction mixture was stirred for 15 min at ambient temperature and then concentrated, and crude (S)-2-((R)-2-aminopropanamido)-3-(4-methoxyphenyl)-N-((S)-1-((R)-2-methyloxiran-2-yl)-1-oxo-3-phenylpropan-2-yl)propanamide TFA salt was carried forward without further purification. MS (EI) for C₂₇H₃₇F₃N₃O₇, found 470.3 (MH⁺).

(S)-2-((R)-2-Aminopropanamido)-3-(4-methoxyphenyl)-N-((S)-1-((R)-2-methyloxiran-2-yl)-1-oxo-3-phenylpropan-2-yl)propanamide TFA salt (2.02 g, 3.67 mmol, 1.00) was dissolved in DMF (10 mL) and cooled to 0 °C. N-Ethyl-N-isopropylpropan-2-amine (1.50 g, 11.6 mmol, 3.00) was added, and the solution was stirred for 5 min. 3-Methyl-1H-indene-2-carboxylic acid (0.741 g, 4.25 mmol, 1.10) was added, followed by HATU (1.62 g, 4.25 mmol, 1.10) over 2 min. The resulting solution was stirred at 0 °C for 10 min. Brine was added, and the resulting solution was extracted with ethyl acetate. The organic phase washed with brine (3×) and was subsequently dried over sodium sulfate, filtered, and the filtrate was concentrated under vacuum. The residue was purified by column chromatography (0–100% heptane/ethyl acetate) to provide 4 (0.13 g, 0.22 mmol, 62% yield). ¹H NMR (400 MHz, DMSO-d₆) δ 8.42 (d, J = 7.2 Hz, 1H), 8.01 (d, J = 8.7 Hz, 1H), 7.71 (d, J = 7.2 Hz, 1H), 7.57–7.44 (m, 2H), 7.40–7.13 (m, 4H), 7.07 (d, J = 8.6 Hz, 2H), 6.81–6.59 (m, 2H), 4.65–4.55 (m, 1H), 4.47 (td, J = 9.3, 4.0 Hz, 1H), 4.35 (m, 1H), 3.66 (m, 2H), 3.62 (s, 3H), 3.22 (d, J = 5.3 Hz, 1H), 3.01–2.89 (m, 3H), 2.77 (dd, J = 13.9, 9.2 Hz, 1H), 2.71–2.56 (m, 1H), 2.39 (t, J = 2.3 Hz, 3H), 1.34 (s, 3H), 1.09 (d, J = 7.1 Hz, 3H); ¹³C NMR (125 MHz, CDCl₃): δ 208.3, 172.7, 171.9, 165.6, 158.3, 145.8, 145.7, 142.7, 137.7, 133.7, 130.8, 129.9, 129.6, 128.9, 127.3, 127.1 (2), 124.3, 121.0, 113.8, 59.6, 55.4, 53.8, 53.2, 52.1, 49.2, 38.7, 37.2, 36.0, 18.5, 16.8, 12.4. HRMS (m/z): [M]⁺ calcd for C₃₆H₄₀N₃O₆, 610.2917; found, 610.2929.

N-((R)-1-(((S)-3-(4-Methoxyphenyl)-1-((S)-1-((R)-2-methyloxiran-2-yl)-1-oxo-3-phenylpropan-2-yl)amino)-1-oxopropan-2-yl)amino)-1-oxopropan-2-yl)cyclohexanecarboxamide (5). The title compound was prepared in analogy to 4. ¹H NMR (400 MHz, DMSO-d₆) δ 8.41 (d, J = 7.1 Hz, 1H), 7.94 (d, J = 8.6 Hz, 1H), 7.75 (d, J = 7.3 Hz, 1H), 7.33–7.16 (m, 5H), 7.07 (d, J = 8.7 Hz, 2H), 6.77 (d, J = 8.7 Hz, 2H), 4.63–4.53 (m, 1H), 4.47–4.37 (m, 1H), 4.16 (q, J = 7.2 Hz, 1H), 3.69 (s, 3H), 3.21 (d, J = 5.3 Hz, 1H), 2.99–2.85 (m, 2H), 2.81–2.71 (m, 1H), 2.57 (dd, J = 13.7, 10.2 Hz, 1H), 2.17–2.08 (m, 1H), 1.72–1.51 (m, 5H), 1.34 (s, 3H), 1.30–1.03 (m, 6H), 0.93 (d, J = 7.1 Hz, 3H); ¹³C NMR (125 MHz, CDCl₃): δ 207.1, 176.4, 172.3, 170.5, 158.7, 136.0, 130.3, 129.3, 128.5, 128.3, 127.0, 114.1, 59.2, 54.2, 52.9, 52.5, 48.7, 45.1, 37.0, 36.7, 29.5, 29.4, 25.7 (2), 25.6, 17.9, 16.5. HRMS (m/z): [M]⁺ calcd for C₃₂H₄₂N₃O₆, 564.3074; found, 564.3068.

(1R,4R)-4-Hydroxy-N-((R)-1-(((S)-3-(4-methoxyphenyl)-1-(((S)-1-((R)-2-methyloxiran-2-yl)-1-oxo-3-phenylpropan-2-yl)amino)-1-oxopropan-2-yl)amino)-1-oxopropan-2-yl)cyclohexanecarboxamide (6). The title compound was prepared in analogy to 4. ¹H NMR (400 MHz, DMSO-d₆) δ 8.41 (d, J = 7.2 Hz, 1H), 7.93 (d, J = 8.7 Hz, 1H), 7.79 (d, J = 7.3 Hz, 1H), 7.37–7.16 (m, 5H), 7.07 (d, J = 8.7 Hz, 2H), 6.77 (d, J = 8.7 Hz, 2H), 4.63–4.54 (m, 1H), 4.50 (d, J = 4.5 Hz, 1H), 4.46–4.37 (m, 1H), 4.16 (m, 1H), 3.69 (s, 3H), 3.25 (m, 3H), 3.01–2.86 (m, 2H), 2.75 (dd, J = 13.9, 9.0 Hz, 1H), 2.57 (dd, J = 13.9, 10.0 Hz, 1H), 2.11–1.95 (m, 1H), 1.80 (m, 2H), 1.63 (m, 2H), 1.338–1.29 (m, 5H), 1.15–1.00 (m, 2H), 0.93 (d, J = 7.1 Hz, 3H); ¹³C NMR (125 MHz, CDCl₃): δ 207.2, 175.6, 172.3, 170.5, 158.7, 135.9, 130.3, 129.3, 128.5, 128.2, 127.0, 114.1, 69.8, 59.2, 55.2, 54.1, 52.9, 52.4, 48.7, 44.0, 37.0, 36.9, 34.6, 27.8, 27.6, 18.0, 16.5; HRMS (m/z): [M]⁺ calcd for C₃₂H₄₂N₃O₇, 580.3023; found, 580.3024.

(1R,4R)-N-((R)-1-(((S)-1-(((S)-3-Cyclobutyl-1-((R)-2-methyloxiran-2-yl)-1-oxopropan-2-yl)amino)-3-(4-methoxyphenyl)-1-oxopropan-2-yl)amino)-1-oxopropan-2-yl)-4-hydroxycyclohexanecarboxamide (7). The title compound was prepared in analogy to 4. ¹H NMR (300 MHz, CDCl₃): δ 7.11 (d, J = 8.4 Hz, 2H), 6.82 (d, J = 9.0 Hz, 2H), 6.76 (m, 1H), 6.52 (m, 1H), 6.33 (m, 1H), 4.44 (m, 1H), 4.39 (m, 2H), 3.79 (s, 3H), 3.56 (m, 1H), 3.23 (d, J = 5.1 Hz, 1H), 2.99 (m, 2H), 2.88 (m, 1H), 2.08 (m, 1H), 2.06–2.02 (m, 4H), 1.99–1.77 (m, 8H), 1.65 (m, 2H), 1.64 (m, 5H), 1.27 (m, 5H); ¹³C NMR (125 MHz, CDCl₃): δ 207.8, 175.6, 172.3, 170.5, 158.7, 130.4, 128.2, 114.0, 69.8, 59.1, 55.3, 54.3, 52.3, 50.6, 48.8, 44.0, 38.2, 37.1, 34.6, 32.6, 31.9, 29.7, 28.7, 28.1, 27.8, 27.7, 18.4, 18.3, 16.7; HRMS (m/z): [M]⁺ calcd for C₃₀H₄₄N₃O₇, 558.3179; found, 558.3196

(1*r*,4*R*)-*N*-((*R*)-1-(((*S*)-1-(((*S*)-3-(Cyclopent-1-en-1-yl)-1-((*R*)-2-methyloxiran-2-yl)-1-oxopropan-2-yl)amino)-3-(4-methoxyphenyl)-1-oxopropan-2-yl)amino)-1-oxopropan-2-yl)-4-hydroxycyclohexanecarboxamide (**8**). The title compound was prepared in analogy to **4**. ¹H NMR (400 MHz, CDCl₃) δ 7.19–7.09 (m, 2H), 6.88–6.71 (m, 2H), 6.53 (d, *J* = 7.7 Hz, 1H), 6.10 (dd, *J* = 12.8, 7.0 Hz, 2H), 5.30 (s, 1H), 4.54 (td, *J* = 7.9, 6.8, 3.4 Hz, 2H), 4.36 (p, *J* = 7.0, 7.0, 7.0 Hz, 1H), 3.78 (s, 3H), 3.61 (td, *J* = 10.8, 10.7, 5.5 Hz, 1H), 3.28 (d, *J* = 5.0 Hz, 1H), 2.97 (qd, *J* = 14.1, 14.0, 14.0, 6.7 Hz, 2H), 2.89 (d, *J* = 5.0 Hz, 1H), 2.45 (s, 1H), 2.36–2.20 (m, 3H), 2.19–2.10 (m, 2H), 2.04 (dt, *J* = 11.7, 3.4, 3.4 Hz, 3H), 1.95–1.69 (m, 4H), 1.58–1.36 (m, 6H), 1.26 (d, *J* = 7.0 Hz, 4H). ¹³C NMR (125 MHz, CDCl₃): δ 207.7, 175.5, 172.3, 170.5, 158.7, 138.7, 130.4, 128.4, 128.3, 114.0, 69.8, 59.2, 55.2, 54.2, 52.2, 50.3, 48.7, 44.0, 37.3, 34.7, 34.6, 32.7, 32.4, 27.8, 27.7, 23.5, 18.5, 16.5. HRMS (*m/z*): [M]⁺ calcd for C₃₁H₄₄N₃O₇, 570.3179; found, 570.3183.

(*S*)-2-(2-(Azepan-1-yl)acetamido)-4-methyl-*N*-((*S*)-1-(((*S*)-1-((*R*)-2-methyloxiran-2-yl)-1-oxo-3-phenylpropan-2-yl)amino)-1-oxo-3-phenylpropan-2-yl)pentanamide (**9**). The title compound was prepared in analogy to **10**. ¹H NMR (400 MHz, DMSO-*d*₆): δ 8.44 (d, *J* = 7.4 Hz, 1H), 8.09 (d, *J* = 8.5 Hz, 1H), 7.58 (d, *J* = 8.9 Hz, 1H), 7.34–7.11 (m, 10H), 4.66–4.47 (m, 2H), 4.31 (q, *J* = 8.1, 7.7 Hz, 1H), 3.18 (d, *J* = 5.2 Hz, 1H), 3.06–2.87 (m, 5H), 2.80–2.63 (m, 2H), 2.63–2.48 (m, 6H), 1.57–1.50 (m, 7H), 1.47–1.39 (m, 1H), 1.36–1.29 (m, 5H), 0.81 (d, *J* = 6.2 Hz, 6H). ¹³C NMR (100 MHz, DMSO-*d*₆): δ 208.15, 171.97, 171.73, 170.19, 138.04, 137.64, 129.64, 129.55, 128.82, 128.46, 127.11, 126.75, 62.21, 59.48, 56.21, 53.66, 52.88, 52.11, 50.73, 42.27, 38.02, 36.02, 28.55, 26.94, 24.74, 23.65, 22.34, 16.77. MS (*m/z*): [M]⁺ calcd for C₃₅H₄₉N₄O₅, 605.37; found 605.52.

(*S*)-2-(2-(Azepan-1-yl)acetamido)-4-methyl-*N*-((*S*)-1-(((*S*)-1-((*R*)-2-methyloxiran-2-yl)-1-oxo-4-(*p*-tolyl)butan-2-yl)amino)-1-oxo-3-phenylpropan-2-yl)pentanamide (**10**). HATU (28.5 g, 75 mmol) and *N*-ethyl-*N*-isopropylpropan-2-amine (36.4 mL, 205 mmol) were added to a solution of BOC-*L*-leucine (15.8 g, 68 mmol) and *L*-phenylalanine benzyl ester (HCl salt, 19.9 g, 68 mmol) in DMF (200 mL) at 0 °C with stirring. The reaction mixture was allowed to warm to room temperature and stirred for 3 h. EtOAc (1 L) and water (1 L) were added, and two layers were separated. The aqueous phase was extracted with EtOAc (300 mL × 3), and the combined organic phases were washed with brine (500 mL × 3), dried over anhydrous Na₂SO₄, and concentrated. The residue was purified by flash column chromatography on silica gel (EtOAc/hexane = 1:4) to afford benzyl (*tert*-butoxycarbonyl)-*L*-leucyl-*L*-phenylalaninate (27.0 g, 84% yield).

TFA (25 mL) was added to a solution of benzyl (*tert*-butoxycarbonyl)-*L*-leucyl-*L*-phenylalaninate (4.95 g, 10.5 mmol) in CH₂Cl₂ (50 mL) at 0 °C. The reaction mixture was allowed to warm to room temperature and stirred for 5 h. The mixture was concentrated to dryness to afford (*S*)-benzyl 2-((*S*)-2-amino-4-methylpentanamido)-3-phenylpropanoate TFA salt (**13**, 5.0 g, ~100% yield), which was used directly for the next step without further purification.

Methyl 2-(azepan-1-yl)acetate (**14**, 1.8 g, 10.5 mmol) was treated with a solution of lithium hydroxide–H₂O (1.0 g, 25 mmol) in water/THF (20 mL/20 mL) for 1 h. THF was removed, and the aqueous phase was acidified to pH = 3–4 with 1 N HCl. The resulting mixture was concentrated to dryness to afford crude 2-(azepan-1-yl)acetic acid (**15**).

2-(Azepan-1-yl)acetic acid (**15**, 10.5 mmol) and **13** (10.5 mmol) were dissolved in DMF (100 mL) and then cooled to 0 °C. HATU (4.4 g, 11.5 mmol) and DIPEA (5.53 mL, 31.5 mmol) were added. The reaction mixture was stirred for 0.5 h and then allowed to warm to room temperature and stirred for 3 h. EtOAc (300 mL) and water (500 mL) were added, and the two layers were separated. The aqueous phase was extracted with EtOAc (200 mL × 3), and the combined organic phases were washed with brine (500 mL × 3), dried over anhydrous Na₂SO₄, and concentrated. The residue was purified by flash column chromatography on silica gel (CH₂Cl₂/

EtOAc = 2:1) to afford benzyl 2-(azepan-1-yl)acetyl-*L*-leucyl-*L*-phenylalaninate (4.8 g, 90% yield).

Benzyl 2-(azepan-1-yl)acetyl-*L*-leucyl-*L*-phenylalaninate (1.0 g, 2 mmol) was dissolved in MeOH (30 mL), and Pd/C (10%, 1 g) was added. The suspension was stirred under a hydrogen atmosphere at room temperature for 2 h. Pd/C was filtered off and washed with MeOH (10 mL). The filtrate and washings were combined and concentrated to dryness to afford 2-(azepan-1-yl)acetyl-*L*-leucyl-*L*-phenylalanine (**16**, 950 mg, quantitative), which was used directly without further purification.

(*S*)-2-Amino-1-((*R*)-2-methyloxiran-2-yl)-4-(*p*-tolyl)butan-1-one TFA salt (**25**, 165 mg, 0.5 mmol) and 2-(azepan-1-yl)acetyl-*L*-leucyl-*L*-phenylalanine (**16**, 238 mg, 0.5 mmol) were dissolved in DMF (13 mL). HATU (205 mg, 0.55 mmol) and DIPEA (0.17 mL) were added at 0 °C with stirring. The reaction mixture was allowed to warm to room temperature and stirred for 3 h. EtOAc (100 mL) and water (100 mL) were added. The organic phase was separated, and the aqueous phase was extracted with EtOAc (50 mL × 3). The combined organic phases were washed with brine (200 mL × 3), dried over anhydrous Na₂SO₄, and concentrated. The residue was purified by silica gel column chromatography (CH₂Cl₂/EtOH/MeOH = 20:10:1) to afford **10** (133 mg, 42% yield). ¹H NMR (400 MHz, DMSO-*d*₆) δ 8.39 (d, *J* = 7.2 Hz, 1H), 8.21 (d, *J* = 8.3 Hz, 1H), 7.62 (d, *J* = 8.8 Hz, 1H), 7.23 (d, *J* = 4.2 Hz, 4H), 7.21–7.13 (m, 1H), 7.07 (s, 4H), 4.65–4.53 (m, 1H), 4.39–4.24 (m, 2H), 3.09 (d, *J* = 5.2 Hz, 1H), 3.04–2.92 (m, 4H), 2.78 (dd, *J* = 14.0, 9.8 Hz, 1H), 2.64 (ddd, *J* = 14.2, 10.0, 4.7 Hz, 1H), 2.53 (d, *J* = 5.0 Hz, 4H), 2.25 (s, 3H), 1.94–1.81 (m, 1H), 1.70–1.61 (m, 1H), 1.58–1.42 (m, 9H), 1.43–1.33 (m, 5H), 0.83 (d, *J* = 6.4 Hz, 6H). ¹³C NMR (100 MHz, DMSO-*d*₆) δ 208.26, 172.13, 171.79, 170.25, 138.18, 135.36, 129.65, 129.39, 128.77, 128.56, 128.51, 126.77, 62.20, 59.40, 56.20, 53.84, 52.10, 51.41, 50.82, 42.36, 37.81, 32.06, 31.54, 28.56, 26.93, 24.76, 23.64, 22.41, 21.18, 16.93. MS (*m/z*): [M]⁺ calcd for C₃₇H₅₃N₄O₅, 633.40; found, 633.61.

(*S*)-*N*-((*S*)-3-(Cyclopent-1-en-1-yl)-1-((*R*)-2-methyloxiran-2-yl)-1-oxopropan-2-yl)-3-(4-methoxyphenyl)-2-((*S*)-2-(2-morpholinoacetamido)propanamido)propanamide (**11**, KZR-177). The title compound was prepared in analogy to KZR-616 (**12**). ¹H NMR (300 MHz, CDCl₃): δ 7.29 (br s, 1H), 7.16 (d, *J* = 8.7 Hz, 2H), 6.83 (d, *J* = 8.7 Hz, 2H), 6.74 (d, *J* = 7.2 Hz, 1H), 6.10 (d, *J* = 7.2 Hz, 1H), 5.33 (s, 1H), 4.56–4.44 (m, 2H), 3.80 (s, 3H), 3.75–3.73 (m, 4H), 3.29 (d, *J* = 4.8 Hz, 1H), 3.00–2.91 (m, 5H), 2.53–2.47 (m, 5H), 2.27–2.16 (m, 5H), 1.90–1.81 (m, 1H), 1.73 (s, 3H), 1.37 (d, *J* = 7.2 Hz, 3H). ¹³C NMR (100 MHz, CDCl₃) δ 208.49, 172.18, 171.52, 168.79, 158.31, 140.00, 130.72, 129.87, 126.86, 113.89, 66.63, 61.73, 59.46, 55.45, 54.14, 53.67, 51.87, 49.92, 47.96, 37.32, 35.11, 32.61, 32.32, 31.51, 29.04, 23.48, 22.62, 19.35, 16.72, 14.51. MS (EI) for C₃₀H₄₂N₄O₇, found 571.4 (MH)⁺.

(**25,3R**)-*N*-((*S*)-3-(Cyclopent-1-en-1-yl)-1-((*R*)-2-methyloxiran-2-yl)-1-oxopropan-2-yl)-3-hydroxy-3-(4-methoxyphenyl)-2-((*S*)-2-(2-morpholinoacetamido)propanamido)propanamide (**12**, KZR-616). A solution of glycine (45.0 g, 0.600 mol) and anisaldehyde (122 g, 0.900 mol) in ethanol (1.5 L) was stirred at ambient temperature, and KOH (82.7 g, 1.47 mol) was added. The reaction mixture was stirred overnight at ambient temperature. The majority of ethanol was removed under vacuum. The resulting residue was dissolved in water (800 mL) and the solution was adjusted to pH = 5 with 4 N aqueous HCl. The resulting mixture was washed with EtOAc (200 mL × 2) to remove any impurities. The aqueous layer was concentrated to a volume of ~400 mL. The mixture was filtered and the filtration cake was washed thoroughly with water (100 mL × 2) and dried to afford racemic 2-amino-3-hydroxy-3-(4-methoxyphenyl)propanoic acid (**30**, 29 g, 23% yield, *threo*-) as a colorless solid which contained 0.4% of the *erythro* diastereomer.

Thionyl chloride (12.3 mL, 169 mmol) was added dropwise to methanol (250 mL) at 0 °C followed by addition of 2-amino-3-hydroxy-3-(4-methoxyphenyl)propanoic acid (**30**, 25.0 g, 118 mol). The reaction mixture was stirred at ambient temperature for 1 h and heated under reflux for 3 h. The mixture was cooled to ambient temperature and then concentrated to dryness. The residue was

purified by flash column chromatography on silica gel (DCM/methanol = 60:1) to afford (2*S*,3*R*)-methyl 2-amino-3-hydroxy-3-(4-methoxyphenyl)propanoate (**31**, 15.7 g, 59% yield, *threo*-) to provide a colorless oil. Further separation by chiral preparative HPLC afforded (2*S*,3*R*)-methyl 2-amino-3-hydroxy-3-(4-methoxyphenyl)propanoate (7.0 g, 45% yield).

To THF (20 mL) was added (2*S*,3*R*)-methyl 2-amino-3-hydroxy-3-(4-methoxyphenyl)propanoate (1.00 g, 4.44 mmol) followed by BOC₂O (1.16 g, 5.33 mmol). The reaction mixture was stirred for 1 h at ambient temperature then concentrated to afford crude (2*S*,3*R*)-2-(*tert*-butoxycarbonylamino)-3-hydroxy-3-(4-methoxyphenyl)propanoate (**33**, 1.44 g, quant) as a colorless solid.

To confirm the stereochemical configuration of **33**, an X-ray crystal of the corresponding amino acid, (2*S*,3*R*)-2-amino-3-hydroxy-3-(4-methoxyphenyl)propanoic acid, was obtained. This material was prepared by deprotecting (2*S*,3*R*)-2-(*tert*-butoxycarbonylamino)-3-hydroxy-3-(4-methoxyphenyl)propanoic acid with TFA to reveal the amino acid (300 mg, 1.42 mmol) following an analogous procedure as referenced below for (2*S*,3*R*)-benzyl 2-((*tert*-butoxycarbonylamino)-3-hydroxy-3-(4-methoxyphenyl)propanoate. The amino acid was diluted with water (5 mL) and methanol (2 mL) and then sealed and heated to reflux for 5 min until complete dissolution of the solid was observed. After allowing to cool to ambient temp over 16 h X-ray quality crystals (200 mg, 67%, colorless flat needles) were provided. ORTEP and coordinates are provided in [Supporting Information Figure 3](#). A mixture of **33** (1.44 g, 4.44 mmol) and LiOH·H₂O (280 mg, 6.66 mmol) in MeOH/THF (30 mL, 1:1) was stirred for 1 h at ambient temperature. EtOAc/water (30 mL/50 mL) was added, and the two phases were separated. The aqueous phase was washed with EtOAc (30 mL × 2) and then acidified with dilute HCl to pH = 5. The resulting mixture was extracted with EtOAc (50 mL × 2). The organics were combined, dried over anhydrous sodium sulfate, and concentrated to afford (2*S*,3*R*)-2-(*tert*-butoxycarbonylamino)-3-hydroxy-3-(4-methoxyphenyl)propanoic acid (0.90 g, 65% yield) as a colorless solid.

Benzyl bromide (4.40 g, 25.7 mmol) was added dropwise to a mixture of (2*S*,3*R*)-2-(*tert*-butoxycarbonylamino)-3-hydroxy-3-(4-methoxyphenyl)propanoic acid (4.00 g, 12.9 mmol) and Cs₂CO₃ (4.20 g, 12.9 mmol) in DMF (80 mL) at 0 °C. The reaction mixture was allowed to warm to ambient temperature and stirred for 1 h. Water (80 mL) was added, and the resulting mixture was extracted with EtOAc (100 mL × 2). The combined extracts were washed with water (100 mL) and brine (100 mL), dried over anhydrous sodium sulfate, and concentrated. The residue was purified by column chromatography (petroleum ether/EtOAc = 10:1 to 4:1) to afford (2*S*,3*R*)-benzyl 2-((*tert*-butoxycarbonylamino)-3-hydroxy-3-(4-methoxyphenyl)propanoate (3.7 g, 66% yield) as a colorless solid.

To (2*S*,3*R*)-benzyl 2-((*tert*-butoxycarbonylamino)-3-hydroxy-3-(4-methoxyphenyl)propanoate (3.0 g, 7.5 mmol) in DCM (30 mL) was added TFA (15 mL), and the mixture was stirred at 0 °C. After 30 min it was diluted with DCM (100 mL). Saturated aqueous NaHCO₃ (100 mL) was added, and the two layers were separated. The aqueous layer was extracted with DCM (100 mL × 2), and the combined organics were dried over anhydrous sodium sulfate and concentrated to afford crude (2*S*, 3*R*)-benzyl 2-amino-3-hydroxy-3-(4-methoxyphenyl)propanoate (2.3 g, quant) as an oil, which was used directly in the next step without further purification.

Sequentially HATU (3.41 g, 8.96 mmol) and DIEA (2.60 mL, 15.0 mmol) were added to a 0 °C solution of (2*S*,3*R*)-benzyl 2-amino-3-hydroxy-3-(4-methoxyphenyl)propanoate (2.30 g, 7.47 mmol) and **29** (1.61 g, 7.47 mmol) in DMF (35 mL). The reaction mixture was allowed to warm to ambient temperature and stirred for 1 h. The mixture was concentrated and the residue was purified by flash column chromatography on silica gel (petroleum ether/EtOAc = 2:1 to 1:2) to afford (2*S*,3*R*)-benzyl 3-hydroxy-3-(4-methoxyphenyl)-2-((*S*)-2-(2-morpholinoacetamido)propanamido)propanoate (2.04 g, 54% yield) as a colorless solid.

To a solution of (2*S*,3*R*)-benzyl 3-hydroxy-3-(4-methoxyphenyl)-2-((*S*)-2-(2-morpholinoacetamido)propanamido)propanoate (2.0 g, 4.0 mmol) in THF (40 mL) was added Pd/C (500 mg, 10%). The

mixture was stirred under a hydrogen atmosphere (1 atm) at ambient temperature overnight and then filtered through a pad of Celite. The filtrate was concentrated under reduced pressure and the residue was washed with EtOAc (10 mL) to afford (2*S*,3*R*)-3-hydroxy-3-(4-methoxyphenyl)-2-((*S*)-2-(2-morpholinoacetamido)propanamido)propanoic acid (1.30 g, 78% yield) as a colorless solid. ¹H NMR (300 MHz, DMSO-*d*₆): δ 8.08 (d, *J* = 8.7 Hz, 1H), 7.74 (d, *J* = 8.4 Hz, 1H), 7.27 (d, *J* = 8.4 Hz, 2H), 6.81 (d, *J* = 8.7 Hz, 2H), 5.10–5.07 (m, 1H), 4.41–4.39 (m, 2H), 3.71 (s, 3H), 3.56–3.55 (m, 4H), 2.97–2.73 (m, 2H), 2.38–2.35 (m, 4H), 1.16 (d, *J* = 6.9 Hz, 3H). MS (EI) for C₁₉H₂₇N₃O₇, found 410.2 (MH)⁺.

Sequentially HATU (1.84 g, 4.80 mmol) and DIEA (0.63 mL, 20 mmol) were added to a 0 °C solution of (2*S*,3*R*)-3-hydroxy-3-(4-methoxyphenyl)-2-((*S*)-2-(2-morpholinoacetamido)propanamido)propanoic acid (1.65 g, 4.00 mmol) and (*S*)-2-amino-3-cyclopentyl-1-((*R*)-2-methyloxiran-2-yl)propan-1-one TFA salt (1.2 g, 4.0 mmol) in DMF (30 mL). The reaction mixture was allowed to warm to ambient temperature and stirred for 30 min. The mixture was concentrated and the residue was purified by column chromatography (petroleum ether/EtOAc = 2:1 to EtOAc) to afford (2*S*,3*R*)-*N*-((*S*)-3-cyclopentyl-1-((*R*)-2-methyloxiran-2-yl)-1-oxopropan-2-yl)-3-hydroxy-3-(4-methoxyphenyl)-2-((*S*)-2-(2-morpholinoacetamido)propanamido)propanamide (1.43 g, 61% yield) as a colorless solid. (2*S*,3*R*)-*N*-((*S*)-3-(Cyclopent-1-en-1-yl)-1-((*R*)-2-methyloxiran-2-yl)-1-oxopropan-2-yl)-3-hydroxy-3-(4-methoxyphenyl)-2-((*S*)-2-(2-morpholinoacetamido)propanamido)propanamide (**12**, KZR-616). ¹H NMR (300 MHz, CDCl₃): δ 7.43 (d, *J* = 7.5 Hz, 1H), 7.29–7.23 (m, 2H), 7.01 (d, *J* = 7.5 Hz, 1H), 6.95 (d, *J* = 7.5 Hz, 1H), 6.84 (d, *J* = 8.7 Hz, 2H), 5.48–5.46 (m, 1H), 5.25–5.22 (m, 1H), 4.63–4.60 (m, 2H), 4.50–4.42 (m, 1H), 3.80 (s, 3H), 3.70–3.66 (m, 4H), 3.28 (d, *J* = 5.1 Hz, 1H), 2.99–2.92 (m, 3H), 2.62–2.22 (m, 10H), 1.89–1.84 (m, 2H), 1.54 (s, 3H), 1.33 (d, *J* = 6.9 Hz, 3H). ¹³C NMR (100 MHz, DMSO-*d*₆) δ 208.13, 172.39, 169.75, 169.13, 158.83, 139.96, 134.44, 128.09, 126.95, 113.51, 72.40, 66.68, 61.86, 59.18, 58.95, 55.48, 53.73, 51.72, 49.18, 48.21, 35.21, 32.81, 32.62, 23.54, 19.06, 16.59. HRMS (*m/z*): [M]⁺ calcd for C₃₀H₄₂N₄O₈, 587.3081, found 587.3065.

(S)-2-((tert-Butoxycarbonyl)amino)-3-cyclobutylpropanoic Acid (20). Methanesulfonyl chloride (85 mL, 1.1 mol) was added dropwise to a solution of cyclobutylmethanol (86.0 g, 1.0 mol) and TEA (206.6 mL, 1.5 mol) in DCM (900 mL) at 0–5 °C. The reaction mixture was allowed to warm to room temperature and stirred for 2 h. Water (900 mL) was added and the organic layer was separated, washed with 2 N aqueous HCl (300 mL), water (600 mL), and brine (300 mL), respectively. The organic solution was dried over anhydrous sodium sulfate and concentrated at 20 °C to afford the corresponding methanesulfonate (180 g).

A mixture of methanesulfonate (180 g, 1.09 mol) and NaI (329 g, 2.19 mol) in acetone (1.5 L) was heated at 60 °C for 12 h and then cooled to room temperature. The mixture was filtered, and the filtration cake was washed with acetone (50 mL × 3). The filtrate and washings were combined and concentrated at 10 °C. The residue (containing salt) was washed with water (200 mL) and brine (200 mL), dried over anhydrous sodium sulfate, and concentrated (10 °C) to afford the crude iodide (**17**, 200 g) as a brown oil, which was used directly without further purification.

Potassium *tert*-butoxide (13.0 g, 0.11 mol) was added in portions to a solution of diethyl 2-acetamidomalonate (23.0 g, 0.10 mol) in DMF (100 mL) while keeping the temperature below 10 °C. After the addition was complete, the suspension was stirred for 0.5 h at 10 °C, and **17** (19.6 g, 0.10 mol) was added dropwise. The slurry was stirred for 10 h at room temperature, and water (500 mL) was added. The resulting mixture was extracted with EtOAc (500 mL × 3). The combine organic phases were washed with saturated aqueous NaHCO₃ (500 mL × 3), 5% aqueous KHSO₄ (500 mL × 3), and brine (300 mL × 1), respectively. The organic phase was dried over anhydrous sodium sulfate and concentrated to afford **18** (18.9 g).

Crude **18** was dissolved in ethanol (100 mL), and 2 N aqueous NaOH (100 mL, 0.20 mol) was added. The solution was heated under reflux for 8 h and then cooled to room temperature. The

organic solvent was removed, and the remaining aqueous solution was washed with ethyl ether (50 mL \times 3) and acidified with 2 N aqueous hydrochloric acid to pH = 3. The resulting mixture was extracted with EtOAc (50 mL \times 6) and the combined organic phases were washed with brine (100 mL \times 1), dried over anhydrous sodium sulfate, and concentrated to afford **19** (7.8 g, 34% yield) which was used directly without further purification.

Aqueous NaOH (1 N, 30 mL) was added dropwise to a suspension of **19** (5.73 g, 31.0 mmol) in water (200 mL) with stirring to pH = 7.5. The mixture was stirred for 30 min at 37 °C and then filtered. L-Acylase (1.0 g) was added to the filtrate, and the mixture was stirred for 40 h at 37 °C. The mixture was cooled to room temperature and purified by ion-exchange resin (732#, 100 g) to afford (S)-2-amino-3-cyclobutylpropanoic acid.

(S)-2-Amino-3-cyclobutylpropanoic acid was dissolved in water and acetone (1:1, 200 mL), and the solution was basified with 2 N aqueous NaOH to pH = 8. BOC₂O (4.0 g, 18.3 mmol) was added, and the reaction mixture was stirred for 12 h at room temperature. The organic solvent was removed, and the remaining aqueous solution was washed with ethyl ether (50 mL \times 3) and acidified with 2 N aqueous hydrochloric acid to pH = 3. The resulting mixture was extracted with EtOAc (50 mL \times 6). The combined organic phases were washed with brine (100 mL \times 1), dried over anhydrous sodium sulfate, and concentrated to afford **20** (3.8 g, 47% yield), which was used directly without further purification. MS (*m/z*): [M]⁺ calcd for C₁₂H₂₁N₄S, 244.15; found 244.15.

(S)-2-(*tert*-Butoxycarbonylamino)-3-cyclopentenylpropanoic Acid (**23**). To a solution of cyclopentanone (55.0 g, 0.665 mol) in DCM (1.3 L) was added Na₂CO₃ (104 g, 0.980 mol), and the mixture was cooled to -20 °C. Trifluoromethanesulfonic anhydride (121 mL, 0.720 mol) was added dropwise. After the addition, the cooling bath was removed and the reaction mixture was stirred at ambient temperature overnight. GC-MS analysis showed the reaction was not complete, and additional trifluoromethanesulfonic anhydride (33 mL, 0.20 mol) was added. The reaction mixture was stirred for another 4 h and then quenched with water (800 mL). The aqueous phase was extracted with DCM (300 mL). The organics were then combined, washed with brine, and concentrated to afford **21** as viscous oil (104 g, 73% yield), which was used in the next step without further purification.

To a suspension of zinc (123 g, 1.90 mol) in DMF (500 mL) was added TMSCl (46 mL) dropwise. The mixture was stirred at ambient temperature for 45 min. The upper clear liquid was removed, and the residue was washed with DMF (200 mL \times 2). The resulting solid was resuspended in DMF (200 mL), and the mixture was cooled to 0 °C. A solution of (R)-methyl 2-((*tert*-butoxycarbonyl)amino)-3-iodopropanoate (104 g, 0.320 mol) in DMF (300 mL) was added. The mixture was stirred at 0 °C under nitrogen for 20 min. The upper clear liquid was removed and added to a solution of **21** (90 g, 0.37 mol) and Pd(dppf)Cl₂ (3.9 g, 4.7 mmol) in DMF (500 mL) dropwise. After addition, the reaction mixture was stirred at 50 °C under nitrogen overnight and then cooled to ambient temperature. Brine (500 mL) was added, and the resulting mixture was extracted with MTBE (300 mL \times 3). The organics were combined, washed with brine, and concentrated. The residue was purified by flash column chromatography on silica gel (petroleum ether/EtOAc = 100:1 to 40:1) to afford (S)-methyl 2-((*tert*-butoxycarbonylamino)-3-cyclopentenylpropanoate (**22**) as viscous oil (62 g, 72% yield). ¹H NMR (300 MHz, CDCl₃): δ 5.48 (br s, 1H), 4.97 (d, *J* = 6.6 Hz, 1H), 4.40–4.43 (m, 1H), 3.74 (s, 3H), 2.46–2.63 (m, 2H), 2.23–2.34 (m, 4H), 1.82–1.93 (m, 2H), 1.45 (s, 9H).

To a solution of **22** (62 g, 0.23 mol) in water/methanol (900 mL, 2:1) was added lithium hydroxide hydrate (19.3 g, 0.460 mol). The reaction mixture was stirred at ambient temperature overnight and then concentrated to remove the majority of methanol. The residue was washed with DCM (400 mL), and the aqueous phase was acidified with diluted HCl to pH = 3–4. The resulting mixture was extracted with DCM (300 mL \times 3). The organic layers were combined and concentrated to afford (S)-2-(*tert*-butoxycarbonylamino)-3-cyclopentenylpropanoic acid (**23**, 56 g, 95% yield) as

viscous oil, which was used in the next step without further purification. ¹H NMR (300 MHz, CDCl₃): δ 10.47 (br. s, 1H), 5.52 (br s, 1H), 4.98 (d, *J* = 8.1 Hz, 1H), 4.40–4.44 (m, 1H), 2.50–2.70 (m, 2H), 2.25–2.34 (m, 4H), 1.79–1.93 (m, 2H), 1.45 (s, 9H).

Starting from the appropriate amino acids the following compounds were synthesized in analogy to **26**.

(S)-2-Amino-1-((R)-2-methyloxiran-2-yl)-4-(*p*-tolyl)butan-1-one (**24**). MS (EI) for C₁₄H₁₉NO₂, found 234.1 (MH⁺).

(S)-2-Amino-3-cyclobutyl-1-((R)-2-methyloxiran-2-yl)propan-1-one (**25**). MS (EI) for C₁₀H₁₇NO₂, found 184.1 (MH⁺).

(S)-2-Amino-3-(cyclopent-1-en-1-yl)-1-((R)-2-methyloxiran-2-yl)propan-1-one (**26**). To a flask charged with **23** (55.0 g, 214 mmol) was added THF/DCM (800 mL, 1:1). The solution was cooled to 0 °C, and ethyl chloroformate (24.5 mL, 257 mmol) and *N*-methylmorpholine (28.4 mL, 257 mmol) were added dropwise sequentially. After addition, the mixture was stirred at 0 °C under nitrogen for 1 h. To another flask charged with *N*,*O*-dimethylhydroxylamine HCl (25.0 g, 256 mmol) was added DCM (400 mL). The mixture was cooled to 0 °C, and TEA (38.7 mL, 278 mmol) was added. The resulting mixture was transferred into the former reaction flask. The reaction mixture was allowed to warm to ambient temperature and stirred overnight. The mixture was quenched with water (500 mL) and the organic phase was washed with water (500 mL), dried over anhydrous sodium sulfate, and concentrated to afford (*S*)-*tert*-butyl (3-(cyclopent-1-en-1-yl)-1-(methoxy(methyl)amino)-1-oxopropan-2-yl)carbamate as colorless oil (60 g, 93%), which was used in the next step without further purification.

To a solution of (*S*)-*tert*-butyl (3-(cyclopent-1-en-1-yl)-1-(methoxy(methyl)amino)-1-oxopropan-2-yl)carbamate (81 g, 0.27 mol) in THF (600 mL) was added freshly prepared prop-1-en-2-ylmagnesium bromide (96.0 mL, 1.08 mol) at 0 °C dropwise. After completion of the addition, the reaction mixture was stirred at 0 °C for 2 h and then quenched with saturated aqueous ammonium chloride (500 mL). The resulting mixture was extracted with EtOAc (400 mL \times 2). The organic phases were combined, dried over anhydrous sodium sulfate, and concentrated. The residue was purified by flash column chromatography on silica gel (petroleum ether/EtOAc = 100:1) to afford (*S*)-*tert*-butyl (1-(cyclopent-1-en-1-yl)-4-methyl-3-oxopent-4-en-2-yl)carbamate as colorless oil (39.3 g, 52% yield).

A solution of (*S*)-*tert*-butyl (1-(cyclopent-1-en-1-yl)-4-methyl-3-oxopent-4-en-2-yl)carbamate (10.0 g, 35.6 mmol) in DMF (180 mL) was cooled to -20 °C, and bleach (54.0 mL, 71.2 mmol, 10%) was added dropwise under nitrogen. The reaction mixture was warmed to 0 °C and stirred for 1.5 h. Water (200 mL) was added, and the mixture was extracted with EtOAc (200 mL \times 2). The organic phases were combined, washed with brine (200 mL \times 2), dried over anhydrous sodium sulfate, and concentrated. The residue, containing a 5.5:1 ratio of epoxide diastereomers, was purified by flash column chromatography on silica gel to afford pure *tert*-butyl ((S)-3-(cyclopent-1-en-1-yl)-1-((R)-2-methyloxiran-2-yl)-1-oxopropan-2-yl)carbamate as viscous oil (5.6 g, 53% yield). ¹H NMR (300 MHz, CDCl₃): δ 4.62 (s, 1 H), 4.91 (d, *J* = 7.5 Hz, 1 H), 4.44–4.37 (m, 1H), 3.29 (d, *J* = 4.8 Hz, 1H), 2.89 (d, *J* = 4.8 Hz, 1H), 2.56–2.52 (m, 1H), 2.29–2.26 (m, 5H), 1.92–1.82 (m, 2H), 1.51 (s, 3H), 1.41 (s, 9H).

To *tert*-butyl ((S)-3-(cyclopent-1-en-1-yl)-1-((R)-2-methyloxiran-2-yl)-1-oxopropan-2-yl)carbamate were added DCM (5 mL) and TFA (5 mL). The reaction mixture was stirred for 15 min at ambient temperature at which time it was concentrated and carried forward without further purification. (S)-2-Amino-3-(cyclopent-1-en-1-yl)-1-((R)-2-methyloxiran-2-yl)propan-1-one TFA salt (**26**) was immediately carried forward into the subsequent step (quant yield). MS (EI) for C₁₁H₁₇NO₂, found 196.1 (MH⁺).

To confirm the stereochemical configuration of **26**, an X-ray crystal of the tosylate salt was obtained. This material was generated by dissolving *p*-toluenesulfonic acid monohydrate (0.454 g, 2.39 mmol) in MTBE (3.5 mL) and adding **26** (0.700 g, 2.39 mmol). After allowing the mixture to stand at ambient temp for 16 h, the mixture

was filtered and dried under vacuum to provide X-ray quality crystals (0.300 g, 34%, colorless needles). ORTEP and coordinates are provided in Supporting Information Figure 2.

(2-Morpholinoacetyl)-L-alanine (29). To 4-(4,6-dimethoxy-1,3,5-triazin-2-yl)-4-methyl-morpholinium chloride (76.1 g, 0.276 mol) and *N*-methylmorpholine (NMM; 32.9 mL, 0.300 mol) were added a 0 °C solution of 2-morpholinoacetic acid (20.0 g, 0.138 mmol) and *L*-alanine benzyl ester hydrochloride (35.7 g, 0.166 mol) in DMF (100 mL) and DCM (200 mL). The reaction mixture was stirred for 4 h at ambient temperature and then concentrated. EtOAc (500 mL) and water (500 mL) was added to the residue. The resulting two layers were separated, and the aqueous phase was extracted with EtOAc (3 × 300 mL). The combined organic layers were washed with brine (3 × 500 mL), dried over anhydrous sodium sulfate, and concentrated. The residue was purified by flash column chromatography on silica gel (DCM/MeOH = 100:3) to afford (*S*)-benzyl 2-(2-morpholinoacetamido)propanoate (**28**, 21.1 g, 50% yield).

To Pd/C (10%, 5.0 g) was added a solution of **28** (20.0 g, 69.0 mmol) in MeOH (200 mL). The mixture was stirred under a hydrogen atmosphere at ambient temperature for 4 h, then it was filtered and rinsed with MeOH (200 mL). The filtrate and washings were combined and concentrated to dryness to afford crude product which was washed with EtOAc (2 × 100 mL) and dried under vacuum to afford (*S*)-2-(2-morpholinoacetamido)propanoic acid (**29**, 12.8 g, 86% yield) as an off-white solid. ¹H NMR (300 MHz, DMSO-*d*₆): δ 7.95 (m, 1H), 4.25 (m, 1H), 3.70 (m, 4H), 3.08 (d, *J* = 15.4 Hz, 2H), 2.40–2.55 (m, 4H), 1.30 (d, *J* = 6.6 Hz, 3H).

Solubility Assay. Compounds were dissolved in 50 mM K phosphate buffer (at least 500 μL) at a targeted concentration of 10 mg/mL by shaking in a 25 °C incubator for 24 h. Visual inspection of the compounds in buffers was carried out. Insoluble compounds were separated from supernatant by centrifugation at 15 000 rpm for 15 min at 25 °C. Supernatant samples were transferred to a fresh plate in duplicate. A 100-fold dilution in DMSO was performed for the supernatants in separate wells. In addition, compound standards were prepared in 100% DMSO at three concentrations (from 100 μg/mL to 4 μg/mL). All the samples were analyzed by UV absorbance on HPLC. The concentration of test compounds in buffers was calculated using a calibration curve generated with standards. Reference compound sulfaphenazole was tested in 50 mM potassium phosphate, pH 7.2 buffer. All samples were analyzed on an Agilent 1100 HPLC instrument using a Waters C18 23 mm × 4 mm column, with UV detection at 220, 254, and 280 nm at a 0.3 mL/min flow rate with a gradient of 0–98% acetonitrile (containing 0.1% TFA) in 0.1% aqueous TFA for 2.2 min.

■ ASSOCIATED CONTENT

Supporting Information

The Supporting Information is available free of charge on the ACS Publications website at DOI: 10.1021/acs.jmedchem.8b01201.

Molecular formula strings (CSV)

Human homology models (PDB)

Figure of ProCISE of MOLT-4 cells following immunoproteasome inhibition by ONX 0914, **8**, KZR-504, and **10**; table of pharmacokinetic measurements of **8**, KZR-504, KZR-616, and ONX 0914 in BALB-C mice; table of hydrolase selectivity panel results and methods; and ORTEP and coordinates of **26** and **33** (PDF)

■ AUTHOR INFORMATION

Corresponding Author

*E-mail: dmcminn@kezarbio.com.

ORCID

Dustin L. McMinn: 0000-0002-9584-7524

Author Contributions

C.K. conceived the project. D.L.M. led the project and conceived compound design. H.W.B.J., D.C.M., and S.B. conceived compound design and synthesized compounds. E.L. and J.L.A. performed biochemical and cell biology experiments. T.M. designed and performed in vivo pharmacology experiments.

Notes

The authors declare the following competing financial interest(s): H.W.B.J., J.L.A., E.L., T.M., A.F., D.L.M., and C.K. are current employees of Kezar Life Sciences, Inc. D.C.M. is an employee of purchaser of Onyx Pharmaceuticals, Amgen Inc.

■ ACKNOWLEDGMENTS

We thank L. Kelly for early project support, Jinhai Wang for pharmacokinetic analysis and Evan Lewis for formulations.

■ ABBREVIATIONS USED

LMP2, low-molecular mass polypeptide-2; MECL-1, multicatalytic endopeptidase complex-like 1; LMP7, low-molecular mass polypeptide-7; HATU, 1-[bis(dimethylamino)methylene]-1*H*-1,2,3-triazolo[4,5-*b*]pyridinium 3-oxide hexafluorophosphate; HBTU, 2-(1*H*-benzotriazol-1-yl)-1,1,3,3-tetramethyluronium hexafluorophosphate; DMTMM, 4-(4,6-dimethoxy-1,3,5-triazin-2-yl)-4-methylmorpholinium chloride; ProCISE, proteasome constitutive/immunoproteasome subunit ELISA; PBMC, peripheral blood mononuclear cell; CAIA, anti-collagen antibody induced arthritis

■ REFERENCES

- (1) Collins, G. A.; Goldberg, A. L. The logic of the 26S proteasome. *Cell* **2017**, *169*, 792–806.
- (2) Groettrup, M.; Kirk, C. J.; Basler, M. Proteasomes in immune cells: more than peptide producers? *Nat. Rev. Immunol.* **2010**, *10*, 73–78.
- (3) Puttapparthi, K.; Elliott, J. L. Non-neuronal induction of immunoproteasome subunits in an ALS model: Possible mediation by cytokines. *Exp. Neurol.* **2005**, *196*, 441–451.
- (4) Egerer, T.; Martinez-Gamboa, L.; Dankof, A.; Stuhlmüller, B.; Dörner, T.; Krenn, V.; Egerer, K.; Rudolph, P. E.; Burmester, G.; Feist, E. Tissue-specific up-regulation of the proteasome subunit β5i (LMP7) in Sjögren's syndrome. *Arthritis Rheum.* **2006**, *54*, 1501–1508.
- (5) Visekruna, A.; Slavova, N.; Dullat, S.; Gröne, J.; Kroesen, A.; Ritz, J.; Buhr, H.; Steinhoff, U. Expression of catalytic proteasome subunits in the gut of patients with Crohn's disease. *J. Colorectal Dis.* **2009**, *24*, 1133–1139.
- (6) Manasanch, E. E.; Orłowski, R. Z. Proteasome inhibitors in cancer therapy. *Nat. Rev. Clin. Oncol.* **2017**, *14*, 417–433.
- (7) Dimopoulos, M. A.; Goldschmidt, H.; Niesvizky, R.; Joshua, D.; Chng, W.; Oriol, A.; Orłowski, R. Z.; Ludwig, H.; Facon, T.; Hajek, R.; Weisel, K.; Hungria, V.; Minuk, L.; Feng, S.; Zahnten-Kumeli, A.; Kimball, A. S.; Moreau, P. Carfilzomib or bortezomib in relapsed or refractory multiple myeloma (ENDEAVOR): an interim overall survival analysis of an open-label, randomised, phase 3 trial. *Lancet Oncol.* **2017**, *18*, 1327–1337.
- (8) Alexander, T.; Sarfert, R.; Klotsche, J.; Kühl, A. A.; Rubbert-Roth, A.; Lorenz, H.; Rech, J.; Hoyer, B. F.; Cheng, Q.; Waka, A.; Taddeo, A.; Wiesener, M.; Schett, G.; Burmester, G.; Radbruch, A.; Hiepe, F.; Voll, R. E. The proteasome inhibitor bortezomib depletes plasma cells and ameliorates clinical manifestations of refractory systemic lupus erythematosus. *Ann. Rheum. Dis.* **2015**, *74*, 1474–1478.

- (9) Wang, Y.; Zhou, W.; Zhang, Z. Successful treatment of warm-type haemolytic anaemia with bortezomib in a rituximab-failed systemic lupus erythematosus patient. *Rheumatology* **2015**, *54*, 194–195.
- (10) Zhang, H.; Liu, Z.; Huang, L.; Hou, J.; Zhou, M.; Huang, X.; Hu, W.; Liu, Z. The short-term efficacy of bortezomib combined with glucocorticoids for the treatment of refractory lupus nephritis. *Lupus* **2017**, *26* (9), 952–958.
- (11) Mazepa, M. A. Bortezomib induces clinical remission and reduction of ADAMTS13 inhibitory antibodies in relapsed refractory idiopathic thrombotic thrombocytopenic purpura. *Br. J. Haematol.* **2014**, *164*, 888–902.
- (12) Jakez-Ocampo, J.; Atisha-Fregoso, Y.; Llorente, L. Refractory primary Sjögren syndrome successfully treated with bortezomib. *J. Clin. Rheumatol.* **2015**, *21*, 31–32.
- (13) Muchamuel, T.; Basler, M.; Aujay, M. A.; Suzuki, E.; Kalim, K. W.; Lauer, C.; Sylvain, C.; Ring, E. R.; Shields, J.; Jiang, J.; Shwonek, P.; Parlati, F.; Demo, S. D.; Bennett, M. K.; Kirk, C. J.; Groettrup, M. A selective inhibitor of the immunoproteasome subunit LMP7 blocks cytokine production and attenuates progression of experimental arthritis. *Nat. Med.* **2009**, *15*, 781–788.
- (14) Basler, M.; Mundt, S.; Muchamuel, T.; Moll, C.; Jiang, J.; Groettrup, M.; Kirk, C. J. Inhibition of the immunoproteasome ameliorates experimental autoimmune encephalomyelitis. *EMBO Mol. Med.* **2014**, *6*, 226–238.
- (15) Basler, M.; Dajee, M.; Moll, C.; Groettrup, M.; Kirk, C. J. Prevention of experimental colitis by a selective inhibitor of the immunoproteasome. *J. Immunol.* **2010**, *185*, 634–641.
- (16) Ichikawa, H. T.; Conley, T.; Muchamuel, T.; Jiang, J.; Lee, S.; Owen, T.; Barnard, J.; Nevarez, S.; Goldman, B. I.; Kirk, C. J.; Looney, R. J.; Anolik, J. H. Beneficial effect of novel proteasome inhibitors in murine lupus via dual inhibition of type I interferon and autoantibody-secreting cells. *Arthritis Rheum.* **2012**, *64*, 493–503.
- (17) Huber, E. M.; Basler, M.; Schwab, R.; Heinemeyer, W.; Kirk, C. J.; Groettrup, M.; Groll, M. Immuno- and constitutive proteasome crystal structures reveal differences in substrate and inhibitor specificity. *Cell* **2012**, *148*, 727–738.
- (18) Muchamuel, T.; Basler, M.; Aujay, M. A.; Suzuki, E.; Kalim, K. W.; Lauer, C.; Sylvain, C.; Ring, E. R.; Shields, J.; Jiang, J.; Shwonek, P.; Parlati, F.; Demo, S. D.; Bennett, M. K.; Kirk, C. J.; Groettrup, M. A selective inhibitor of the immunoproteasome subunit LMP7 blocks cytokine production and attenuates progression of experimental arthritis. *Nat. Med.* **2009**, *15*, 781–788.
- (19) Kisselev, A. F.; van der Linden, W. A.; Overkleeft, H. S. Proteasome inhibitors: an expanding army attacking a unique target. *Chem. Biol.* **2012**, *19*, 99–115.
- (20) Federspiel, J. D.; Codreanu, S. D.; Goyal, S.; Albertolle, M. E.; Lowe, E.; Teague, J.; Wong, H.; Guengerich, F. P.; Liebler, D. C. Specificity of protein covalent modification by the electrophilic proteasome inhibitor carfilzomib in human cells. *Mol. Cell. Proteomics* **2016**, *15*, 3233–3242.
- (21) Johnson, H. W. B.; Anderl, J. L.; Bradley, E. K.; Bui, J.; Jones, J.; Arastu-Kapur, S.; Kelly, L. M.; Lowe, E.; Moebius, D. C.; Muchamuel, T.; Kirk, C.; Wang, Z.; McMinn, D. Discovery of highly selective inhibitors of the immunoproteasome low molecular mass polypeptide 2 (LMP2) subunit. *ACS Med. Chem. Lett.* **2017**, *8*, 413–417.
- (22) Parlati, F.; Lee, S. J.; Aujay, M.; Suzuki, E.; Levitsky, K.; Lorens, J. B.; Micklem, D. R.; Ruurs, P.; Sylvain, C.; Lu, Y.; Shenk, K. D.; Bennett, M. K. Carfilzomib can induce tumor cell death through selective inhibition of the chymotrypsin-like activity of the proteasome. *Blood* **2009**, *114*, 3439–3444.
- (23) Huber, E. M.; Heinemeyer, W.; de Bruin, G.; Overkleeft, H. S.; Groll, M. A humanized yeast proteasome identifies unique binding modes of inhibitors for the immunosubunit $\beta 5i$. *EMBO J.* **2016**, *35*, 2602–2613.
- (24) de Bruin, G.; Huber, E. M.; Xin, B. T.; van Rooden, E. J.; Al-Ayed, K.; Kim, K. B.; Kisselev, A. F.; Driessen, C.; van der Stelt, M.; van der Marel, G. A.; Groll, M.; Overkleeft, H. S. Structure-based design of $\beta 1i$ or $\beta 5i$ specific inhibitors of human immunoproteasomes. *J. Med. Chem.* **2014**, *57*, 6197–6209.
- (25) Lee, S. J.; Levitsky, K.; Parlati, F.; Bennett, M. K.; Arastu-Kapur, S.; Kellerman, L.; Woo, T. F.; Wong, A. F.; Papadopoulos, K. P.; Niesvizky, R.; Badros, A. Z.; Vij, R.; Jagannath, S.; Siegel, D.; Wang, M.; Ahmann, G. J.; Kirk, C. J. Clinical activity of carfilzomib correlates with inhibition of multiple proteasome subunits: application of a novel pharmacodynamic assay. *Br. J. Haematol.* **2016**, *173*, 884–895.
- (26) Kalim, K. W.; Basler, M.; Kirk, C. J.; Groettrup, M. Immunoproteasome subunit LMP7 deficiency and inhibition suppresses Th1 and Th17 but enhances regulatory T cell differentiation. *J. Immunol.* **2012**, *189*, 4182–4193.
- (27) Demo, S. D.; Kirk, C. K.; Aujay, M. A.; Buchholz, T. J.; Dajee, M.; Ho, M. N.; Jiang, J.; Laidig, G. J.; Lewis, E. R.; Parlati, F.; Shenk, K. D.; Smyth, M. S.; Sun, C. M.; Vallone, M. K.; Woo, T. M.; Molineaux, C. J.; Bennett, M. K. Antitumor activity of PR-171, a novel irreversible inhibitor of the proteasome. *Cancer Res.* **2007**, *67*, 6383–6391.
- (28) Singh, J.; Petter, R. C.; Baillie, T. A.; Whitty, A. The resurgence of covalent drugs. *Nat. Rev. Drug Discovery* **2011**, *10*, 307–317.
- (29) A Phase 1b/2 Study of KZR-616 in Patients With Systemic Lupus Erythematosus With and Without Nephritis (2018). Retrieved from <https://clinicaltrials.gov>, identification no. NCT03393013 (accessed August 7, 2018).
- (30) (a) McMinn, D.; Johnson, H.; Bowers, S.; Moebius, D. C. Tripeptide Epoxyketone Protease Inhibitors. PCT Int. Appl. WO 2014152134A1, 2014. (b) McMinn, D.; Johnson, H.; Bowers, S.; Moebius, D. C. Tripeptide Epoxy Ketone Protease Inhibitors. U.S. Patent 9,434,761 B2, Nov 11, 2014.
- (31) Shenk, K.; Parlati, F.; Zhou, H.-J.; Sylvain, C.; Smyth, M.; Bennett, M.; Laidig, G. Preparation of Peptide Epoxyketones as Selective Immunoproteasome Inhibitors. U.S. Patent Application 20070293465 A1, 2007.
- (32) Zhou, H.-J.; Aujay, M. A.; Bennett, M. K.; Dajee, M.; Demo, S. D.; Fang, Y.; Ho, M. N.; Jiang, J.; Kirk, C. J.; Laidig, G. J.; Lewis, E. R.; Lu, Y.; Muchamuel, T.; Parlati, F.; Ring, E.; Shenk, K. D.; Shields, J.; Shwonek, P. J.; Stanton, T.; Sun, C. M.; Sylvain, C.; Woo, T. M.; Yang, J. Design and synthesis of an orally bioavailable and selective peptide epoxyketone proteasome inhibitor (PR-047). *J. Med. Chem.* **2009**, *52*, 3028–3038.